Chem. Mater. **2008,** *20,* 649–666

Morphological Control in Colloidal Crystal Templating of Inverse Opals, Hierarchical Structures, and Shaped Particles[†]

Andreas Stein,* Fan Li, and Nicholas R. Denny

Department of Chemistry, University of Minnesota, 207 Pleasant St. S.E., Minneapolis, Minnesota 55455

Received July 30, 2007. Revised Manuscript Received October 17, 2007. Accepted October 18, 2007

Inverse opals or three-dimensionally ordered macroporous (3DOM) materials, prepared by colloidal crystal templating (CCT) methods, possess distinctive structural features that are important for the design of photonic crystals, sensors, power sources, catalysts, and various other applications. In the past decade, vast progress has been made in shaping these materials at various length scales. It is now possible to prepare 3DOM materials in a variety of simple and complex compositions, in which pore sizes, pore shapes, and skeletal geometries can be adjusted statically and sometimes even dynamically to alter the physical properties of the material. Hierarchical pore structures can be achieved by combining CCT with additional templating techniques. Furthermore, shaped porous nanoparticles may be synthesized using CCT methods. This review will highlight recent advances in controlling both the internal structure of inverse opals and their external morphology, enhancing compositional complexity, endowing these solids with functionality, and incorporating them in integrated functional systems.

1. Introduction

Inverse opals sparkle in many colors.[1,2] Their basic architectures are simple and beautiful (Figure 1).[3–6] Conceptually, their preparation is straightforward and quite general.[7–9] But these three-dimensionally ordered macroporous (3DOM) solids have captured the interest of scientists and engineers for more reasons than their visual appeal. Now, after one decade of research on colloidal crystal templating methods to produce inverted opal structures, advancements in synthetic techniques driven by the demands of potential applications have led to big strides in the structural and compositional complexity of these materials. Furthermore, a number of interesting properties have been discovered for inverse opals that derive from their special structural features. In the future, one can expect societal benefits from these and related materials in the realms of communications, energy conversion and storage, environmental remediation, and health. This review will highlight recent progress in controlling morphologies of 3DOM materials at different length scales and illustrate the effects of structural and compositional variations on materials properties using literature examples that target specific applications.

Inverse opals derive their name from the templates used to mold these structures: uniform, spherical, colloidal particles assembled into crystalline arrays that resemble natural opals. Most commonly, silica or polymer spheres are used for the colloidal crystal template, making colloidal crystal templating (CCT) a "hard templating" method. Unlike most natural hard templates, such as bioskeletons, viruses, or plant components, this template boasts a high degree of periodicity in three dimensions, which is also translated into the replica 3DOM structure. To prepare these periodic pore structures, void spaces between spheres in the colloidal crystal template are infiltrated by any type of fluid that penetrates the template and can be converted into a solid. Removal of the templating spheres leaves a solid skeleton that surrounds the air holes left in the original locations of the spheres (Figure 2, top). In general, silica spheres are removed by etching with hydrofluoric acid and polymer spheres by dissolution in appropriate solvents or, more frequently, by calcination or pyrolysis—processes that not only open up the macropore spaces, but also steer the

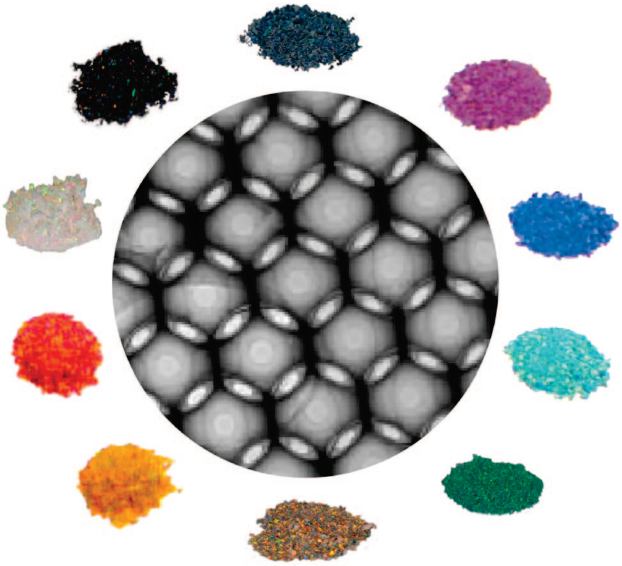

Figure 1. TEM image of 3DOM silica, surrounded by 3DOM samples whose colors and opalescence originate from diffraction by regularly spaced macropores. Clockwise from top: 3DOM TiO_2, three 3DOM ZrO_2 samples with increasing macropore sizes, 3DOM NiO, 3DOM ZrO_2, two 3DOM ZrO_2 samples whose pores are filled with methanol, 3DOM SiO_2, and 3DOM carbon.[2]

---

* Corresponding author phone: 001-612-624-1802; fax: 001-612-626-7541; e-mail: stein@chem.umn.edu.

[†] Part of the "Templated Materials Special Issue".

10.1021/cm702107n CCC: $40.75

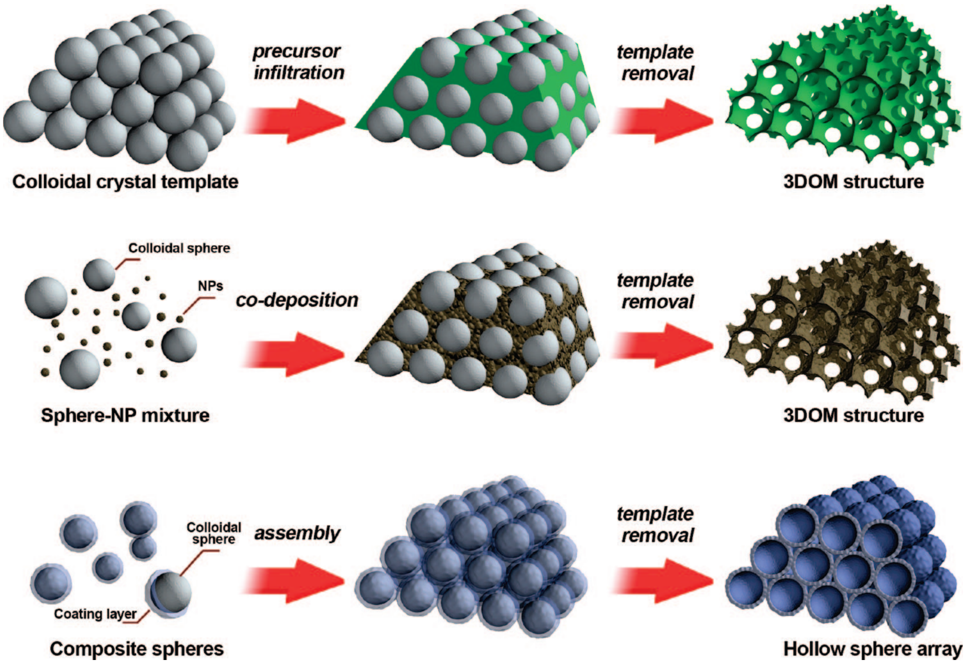

Figure 2. Three methods of preparing periodic macroporous structures by colloidal crystal templating. Top: A preformed colloidal crystal is infiltrated with precursor material which is processed to form the 3DOM structure after removal of the template. Middle: Uniform templating spheres and nanoparticles (NPs) are codeposited to form a 3DOM structure after template removal. Bottom: Core-shell structures are assembled into periodic arrays, forming close-packed hollow shells.

skeleton formation and influence the local architecture of the skeleton.

As inverse replicates of the typically face-centered cubic (*fcc*) opaline template, the skeletal walls surround regular macropores that are interconnected through windows at the points where the original spheres touched. For an *fcc* template, this corresponds to 12 windows per macropore. Most studies have employed colloidal spheres with diameters in the submicrometer range, so that the resulting voids (macropores) have similar dimensions, although in many cases their diameters are reduced by 10–30% due to shrinkage of the precursor or the template. With these dimensions, the walls have thicknesses corresponding to tens of nanometers. As a result, they can exhibit the properties of nanoparticles, including high surface-to-volume ratios and unique confinement properties. The smallest limit of the templating sphere size to achieve ordered pores has recently been tested in the case of carbon templated from silica colloids.[10] In that system, the cutoff for periodicity appeared to be near 50 nm, although it depended to some extent on the carbon precursor. Many of the concepts presented here may be translated to much larger spheres, but in that case, the advantages derived from nanometer dimensions may be lost.

CCT methods lend themselves to the preparation of many compositions of ordered macroporous materials. Since the major requirements for a successful synthesis are efficient infiltration of the template by a precursor and conversion of the precursor into the desired solid phase, a wide range of chemical techniques has been employed to achieve the desired structures and compositions. 3DOM structures have been synthesized as pure elements, alloys, salts, binary and more complex oxides and other chalcogenides, pnictides, polymers, and composites. In addition to the infiltration of colloidal crystal templates, two alternate assembly processes for ordered macroporous materials should be mentioned. One method, the simultaneous assembly of small nanoparticles with larger colloidal spheres, produces similar structures to those described above when nanoparticles fill the voids between the templating spheres during assembly (Figure 2, middle).[11–13] This method can be advantageous if nanoparticles of a desired composition are more easily prepared before templating, so that compositional homogeneity is maintained in the structured product. The other alternate method involves the preparation of core–shell structures that are subsequently assembled into a colloidal crystal (Figure 2, bottom).[14–16] This method provides good control over the shell thickness, which translates directly into the wall thickness of the assembled 3DOM material. However, thicker shells remain relatively closed after removal of the cores, so that the interconnectedness of macropores is lower than that achieved by infiltration methods.

Proposed applications of 3DOM materials derive benefits from different features of this architecture. If the regular skeletal structure is on the length scale of optical wavelengths, it leads to important photonic properties targeted in photonic band gap materials, which are useful to manipulate or guide light transmission for optical communication, photocatalysis, and next-generation integrated circuits. The resulting optical properties are also of interest for pigments, camouflage applications, and sensors. The bicontinuous nature of the structure (an interconnected solid skeleton and an interconnected pore system) can serve transport applications through both phases: transport of the guest molecules in the macropore phase and of ions or electrons in the solid phase. These properties are useful in fuel cells, microreactors, electrochemical cells, catalysis, and separations. The relatively large macropore spaces provide sufficient room to design structural complexity into the material by functionalization of the walls with molecular groups, clusters, polymers, and nanoparticles. The walls themselves, as noted earlier, feature the special properties of nanometer-sized materials: optical, electronic, and magnetic properties modified by confinement effects. By combining CCT with other soft or hard templating methods, the wall structure itself can be altered to produce materials with hierarchical pore systems. Beyond defining structure, the solid matrix can participate in chemical reactions. The high surface-to-volume ratios of the skeleton can enhance surface reactions, but they can also be detrimental in applications where the resulting high reactivity causes a loss of the structural integrity.

Several review articles on colloidal crystal formation,[17–24] as well as colloidal crystal templating, inverse opals, or 3DOM materials, have appeared in the past few years.[25–31] A comprehensive review was prepared by one of the authors only a year ago.[32] Therefore, the present paper will concentrate largely on progress made recently in controlling both the internal structure of inverse opals and their external morphology, enhancing compositional complexity, endowing these solids with functionality, and incorporating them in integrated functional systems.

2. Compositional Control in 3DOM Structures

Because of the myriad of colloidal crystal infiltration or assembly methods, the list of possible compositions for 3DOM materials is open-ended.[32] Many different compositions have already been prepared, and additions of new ones merely for the purpose of synthetic demonstrations may be of limited utility. However, in many cases, 3DOM structures with new compositions are designed to serve specific applications or provide special physicochemical properties, and for these reasons, synthetic flexibility becomes valuable. Some of the synthetic techniques that have been reviewed previously include solution and melt infiltration, sol–gel chemistry, in situ polymerization, electrodeposition, chemical bath deposition, chemical vapor deposition (CVD), plasma-enhanced CVD, physical vapor deposition, pulsed laser deposition (PLD), atomic layer deposition (ALD), infiltration with nanoparticles, co-deposition of template particles with nanoparticles, and assembly of core–shell structures. As noted above, the precursors must be able to penetrate the colloidal crystal and react inside to be transformed into the desired solid phase. The product phase needs to survive the template removal conditions and ideally, should not deform under those conditions. Infiltration is possible in the gas phase, liquid phase, solution phase, and even with dispersions of nanoparticles. In the case of liquid and solution phase precursors, interfacial interactions, including the wettability of surfaces, are important to guarantee efficient filling of the interstitial space. Often, the use of mixed solvent systems benefits infiltration. Of course, solvents dilute the precursor so that the volume fraction of the product is less than the theoretical 26% expected from using an ideal opal template. When desired, multiple infiltration and drying steps can increase the product volume fraction.

For mixed precursor systems, the solubility of each component must be considered to produce homogeneous product phases. In certain situations, 3DOM structures with compositions as complex as the layered double hydroxide, $Mg_2Al(OH)_6(CO_3)_{0.5}$, are obtained by simple coprecipitation of the ions.[33] Ternary (e.g., $Sm_{0.5}Sr_{0.5}CoO_3$)[34] and even quaternary mixed metal oxides (e.g., $La_{0.7}Ca_{0.3-x}Sr_xMnO_3$)[35] have been synthesized with inverse opal structures. Common chelating agents can help maintain the stoichiometry in complex compositions. Recently, spinel-type mixed 3DOM iron oxides of the type MFe_2O_4 (M = Zn, Ni, Zn_xNi_{1-x}, Co)[36] and perovskite 3DOM $La_{1-x}Sr_xFeO_3$[37] were synthesized using metal nitrates with an ethylene glycol−methanol mixed solvent for precursors. Mixed metal glyoxylate salts are formed by in situ nitrate oxidation at low temperatures before calcination. Thus, multiple transition metals can be incorporated in the skeletal structure with controlled ratios. The amorphous products obtained after template removal had shell structures, but these converted to skeleton structures upon crystallization of the products. This solvent method is more suitable for mixed metal oxides than an older oxalate precipitation method[38] if the solubility of the metal oxalates differs widely. In syntheses of other complex oxides, such as the ternary oxide 3DOM $CsAlTiO_4$[39] or 3DOM $LiCoO_2$,[40] it is challenging to maintain the desired stoichiometry during the synthesis, while keeping the periodic 3DOM structure. Often, high-temperature sintering results in structural collapse or a loss of one or more components, limiting the maximum processing temperature. However, additives that hinder grain growth can help to maintain the ordered pore structure.[40] For example, in the binary oxide 3DOM $Ti_{1-x}Ta_xO_{2+x/2}$ (x between 0.025 and 0.075), Ta_2O_5 doping impeded grain growth of the anatase phase within the wall skeleton and more than doubled the Brunauer−Emmett−Teller surface area of the material, leading to improved photocatalytic activity in the degradation of an aqueous–organic dye.[41]

PLD provides another route for achieving complex compositions by transferring a complex material from a target unto a substrate. However, with this line-of-sight technique, the product does not penetrate deeply into the template. Upon PLD of $CaCu_3Ti_4O_{12}$ onto a thin layer of poly(methyl methacrylate) (PMMA) spheres, the complex oxide formed only on the top layer of the spheres, producing a monolayer of hollow hemispheres.[42] Nonetheless, in sensitivity comparisons between the templated films and similarly prepared nontemplated films, the porous film exhibited remarkably enhanced sensitivity and reversible responses for H_2 gas at temperatures between 200 and 400 °C.

Well-defined compositional gradients in inverted opal walls are possible at an atomic level through ALD. This technique has been used, for example, to fabricate inverse opals with multiple layers of titania and ZnS/Mn to incorporate a luminescing layer within the higher-refractive-index titania phase.[43] Compositional gradients at a slightly larger length scale can be achieved within a 3DOM structure through surface modification of the macroporous structure either during or after the synthesis. The internal surfaces of conductive materials, such as 3DOM carbon, can be coated by electrochemical deposition. For example, an ultrathin conformal layer of an insulating polymer was deposited on 3DOM carbon by self-limiting electrooxidation.[44] Perhaps a more general technique that applies to conducting and nonconducting pore surfaces is layer-by-layer growth,[45,46] which has been applied in order to deposit titania nanoparticle layers onto 3DOM carbon pore walls.[47] If nanoparticles are instead incorporated during the skeletal wall preparation, they may serve as reinforcing agents, as was demonstrated for composites of macroporous chiral polyaniline with titania nanoparticles.[48] The choice of placing nanoparticles either within the wall, on the wall surface, or in the void spaces is particularly important in photonic crystal structures that contain quantum dots as internal sources of light emission.[49] Nanoparticles deposited on the surface may be embedded in the walls by deposition of another layer. As an example, 3DOM ZnO that had been decorated with CdTe nanocrystals as internal light emitters was coated with an additional ZnO layer by CVD.[50] The thickness of the extra layer influenced the position of the photonic features; spontaneous emission from the CdTe quantum dots was inhibited or enhanced, depending of their relative position to the pseudogap, which was controllable by the filling fraction of ZnO.

Several interesting examples in the literature have shown that compositional modification is also possible through modification of the template, using particle transfer processes. When a silica-based colloidal crystal template film is gold-sputtered, infiltrated with polystyrene (PS) to form a membrane, and then etched to remove the silica, the gold is transferred to the polymer walls.[51] There, the gold can act as a seed layer for electroless desposition of additional gold. Because sputtering is a line-of-sight technique, it does not allow for deep penetration of gold seeds beyond the top layers. The structural integrity therefore deteriorates quickly for lower-lying layers. More uniform gold distributions in a 3DOM polymer film may be possible by coating amine-functionalized silica spheres with gold nanoparticles, infiltrating the colloidal crystal with polystyrene, and removing silica.[52,53] Such transfer processes are not limited to gold but have also been demonstrated for silver particles. When a silica opal is soaked in Tollens solution, silver nanoparticles decorate the sphere surfaces and are transferred to a polystyrene layer after infiltration with a polymer precursor, polymerization, and HF etching of the spheres.[54] Transfer is possible from polystyrene to silica as well, when sulfate-functionalized polystyrene spheres are coated with silver nanoparticles, infiltrated with tetraethoxysilane, and calcined.[55]

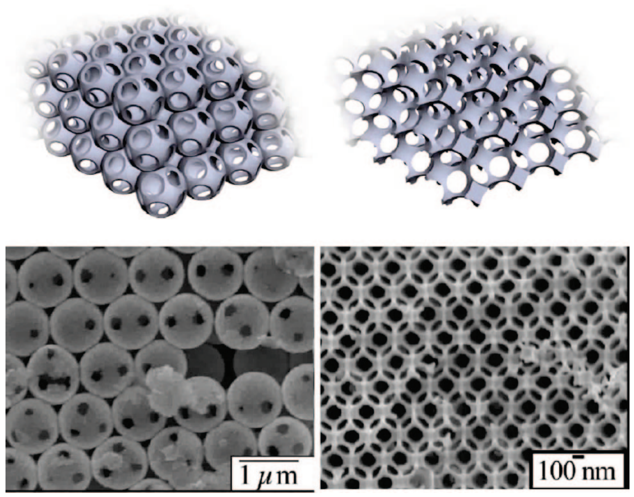

Figure 3. Schematic diagrams and scanning electron microscopy (SEM) images of surface-templated (left) and volume-templated materials (right). The SEM images correspond to tungsten inverse opals prepared by chemical vapor deposition (left) and wet chemical methods (right). They are reprinted with permission from ref 63, Denny et al. “Synthetic approaches toward tungsten photonic crystals for thermal emission,” *Proc. of SPIE* **2005**, *6005 (Photonic Crystals and Photonic Crystal Fibers for Sensing Applications)*, 600505–1, copyright Society of Photo-Optical Instrumentation Engineers.

3. Controlling the Templated Wall Structure

While many different 3DOM materials look similar on the length scale of the templated macropores, the wall structure can vary significantly when considered at a higher resolution. Differences in sizes and shapes of windows that interconnect macropores, texture of the walls, thickness of walls, and shapes of interconnecting struts can alter the width of photonic bandgaps in photonic crystals,[56–58] change transport properties of guest species through the pores, and influence the efficiency of surface reactions.[59] Larger windows between adjacent cages increase the transmission of light in metallic photonic crystals.[60] Wall thicknesses impact the conductivity,[61] superconductivity,[62] and magnetic properties of inverse opals as a result of finite size effects. For example, in 3DOM gold with walls thinner than ca. 50 nm, the mean free path of electrons becomes larger than the wall thickness.[61] As a result, the resistance is dominated by surface scattering rather than lattice scattering. This may permit the use of 3DOM gold electrodes with pore diameters less than 500 nm as resistive sensors for the detection of chemisorbed species.[61] If walls are composed of crystalline nanoparticles, the size of these particles affects light scattering properties. For illustration, zirconia inverse opals with very small grains in the skeleton appear strongly colored, but they lose this color if grain sizes exceed a certain limit, leading to secondary light scattering effects.[2] For these reasons, synthetic control over the templated wall structure is critical.

The skeletal shape obtained by CCT depends on the deposition technique and on interactions between wall precursors and the template.[63] If the infiltrating precursor interacts strongly with the spheres, the skeletal walls follow the curvature of the spheres and the product can be truly considered an “inverse opal” with close-packed “air spheres” separated by solid walls (Figure 3). With infiltrating techniques that build up the solid from the sphere surface into the interstitial spaces, access to these spaces becomes closed off after a certain deposition thickness, leaving small holes in addition to the larger air spheres. This kind of “surface templating” process is found in certain electrochemical, chemical vapor, or atomic layer deposition techniques and also when precursors are covalently bonded to the template. As an example, surface-templated polymer and carbon structures are created on silica opal templates using atom transfer radical polymerization (ATRP), a process which grafts polymer brushes directly on the surface of the silica spheres.[64] Products consist of strongly curved shell structures whose thicknesses are controllable via the ATRP time and monomer feeding.

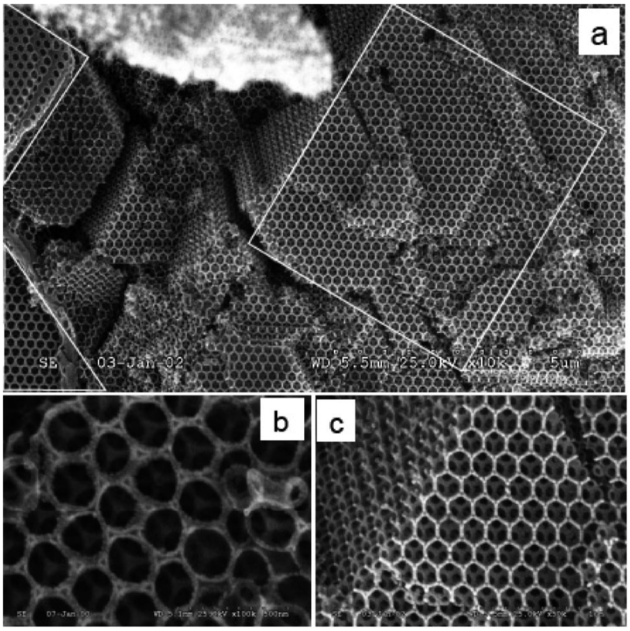

Figure 4. SEM images of 3DOM titania with two kinds of wall structures in the view field (a). Details: (b) shell structure near the surface and (c) rod structure deeper within the sample. Reprinted with permission from ref 67, Dong et al. *Chem. Mater.* **2003**, *15*, 568.

In many solvent-based infiltration techniques, precursor−precursor interactions are stronger than precursor−wall interactions, and the solid fills the bulk of the interstitial space ("volume templating"). If significant volume losses are involved during calcination, the skeleton becomes less curved and can be considered as a scaffold of nodes (in the octahedral and tetrahedral holes of the original *fcc* template) connected by nearly rodlike structures. As a result, windows between macropores are larger in volume-templated structures than in surface-templated products. These seemingly small changes in local structure can have large implications on the optical properties (photonic band structures)[60,65] and transport properties of 3DOM materials.

For sol–gel infiltrations, the dependence of a spherical versus rodlike skeletal structure on reaction parameters is relatively complex, as demonstrated in the case of macroporous titania. Neat or diluted titanium alkoxide precursors have produced both volume-templated[4,66,67] and surface-templated products.[68,69] Different electrostatic interactions between the colloidal crystal template and precursor solutions are likely responsible for the different morphologies. In fact, the wall structure can depend on the location within a sample, skeletal structures being more common in the inner portion of the sample and shell structures more dominant at the surface (Figure 4).[67] This behavior is related to different hydrolysis, condensation, and drying conditions in the various regions. A transformation of a shell structure to a skeletal structure can occur during crystallization of an originally amorphous wall.[36] During thermal sintering of the walls, mass transport from the middle parts of the bridges to the nodal points causes thinning of the struts.[70] If an increased solid volume fraction is desired, for example, to alter the photonic band structure,[58] walls can be thickened by multiple infiltrations of dilute alkoxide.[71] However, this can lead to surface crust formation and blocked macropores. If a surface crust forms, it can be removed by ion milling.[72]

Depending on the extent of infiltration into a colloidal crystal template, one can achieve two different types of architectures, as was demonstrated by CVD of silicon in a silica inverse opal.[73] Inverse opals prepared by partial infiltration with silica produced two independent, isolated networks when used as templates for silicon deposition, one conforming to the macropore surface, the other corresponding to the incompletely filled interstitial sites in the initial template. In contrast, silica inverse opals prepared by complete infiltration maintained a single network, and subsequent silicon infiltration mainly modified the thickness of the walls.

Smooth macropore walls that conform to the templating sphere surface are observed in the case of electrochemically deposited titania.[74] Yet, by electrochemical deposition, it is also possible to attain a complete filling of interstitial space with good "volume templating" and negligible shrinkage, so that the inverse opal resembles the interstitial space very closely.[75] It has been noted that the first layer of templated material from an electrochemical synthesis has a different pore structure from later layers, as a result of the substrate next to the initial layer.[75] Very fine control over conformal coatings on a CCT is provided by ALD. 3DOM multilayer composite films fabricated by ALD are extremely high quality photonic crystal materials with surface-templated pore walls, defect-free domains covering several micrometers, controllable pore wall thicknesses to a precision of 0.5 Å/cycle, and possible high solid-volume filling fractions.[43,72,76] Furthermore, ALD can, in many cases, be applied at low temperatures (e.g., < 80 °C for Al_2O_3 and TiO_2), reducing the thermal requirements on a CCT.[76]

While the diameter of interconnecting windows between macropores depends on the extent of surface versus volume templating, it can also be adjusted by annealing and etching the template. For silica opals, extensive sintering at high temperatures (e.g., 1000 °C for 3 h) produces overlap of spheres with merged necks, which will increase window sizes but reduce wall thicknesses.[56,72] In the case of polymeric colloidal crystal templates, heating the polymer slightly above the glass transition temperature for a few minutes strengthens the template and also causes spheres to merge partially. This process needs to be well controlled, so that pores in the template do not close up completely. Even though openings in the colloidal crystal can become very narrow after annealing, certain techniques, like ALD or CVD, permit infiltration of these interstices. A non-close-packed (NCP) silica colloidal crystal is produced by treating sintered silica opals with HF in a controlled manner to etch away the top surface of the spheres.[77] This yields a more open *fcc* structure, in which spheres are separated by narrow cylindrical rods. It permits easier penetration with precursors for templating and can produce thicker walls with more elongated windows and nanochannel structures.[51] Similar NCP arrays of spheres with interconnecting rods have been reported for PMMA sphere arrays.[78]

Titania inverse opals with very small filling fractions (<6 vol %) were prepared by ALD in strongly sintered silica opals.[72] Backfilling of titania by additional ALD cycles produced cylindrical windows with some depth between neighboring air spheres and permitted excellent control over the filling fraction. A template to produce these types of cylindrical connections can also be prepared by a multistep process, in which a silica layer is deposited on the interior surface of a silica inverse opal by CVD to reduce sizes of the air spheres, and the resulting pore structure is then backfilled with polystyrene.[79] After elimination of silica by etching, a non-close-packed polymer opal film is obtained. The size of the resulting spheres and connectors is controlled by varying the thickness of the deposited silica layer.

An alternate method of tuning pore sizes and wall thicknesses involves ALD of a sacrificial layer (e.g., ZnS or Al_2O_3), whose thickness on the template surface is controlled in the deposition process.[76] The desired material (e.g., TiO_2) is then introduced into the remaining space by additional ALD steps. After removal of the template and the sacrificial layer, a very open skeleton is obtained. Walls can be thickened and window sizes reduced by backfilling with additional dielectric material. The sacrificial layer concept can provide greater precision than strong sintering of the colloidal crystal template.

Annealing of templating polymer spheres has also been applied to two-dimensional membrane structures to tune pore sizes.[80] A 2D colloidal crystal of polystyrene spheres was assembled on a planar substrate that had been spin-coated with a thin layer of polystyrene. Heating of this assembly allowed spheres to penetrate into the PS layer. The degree of penetration depended on the heating temperature and time. The resulting sphere array was infiltrated with additional silicone-based polymer precursor solution, which was polymerized to form solid poly(dimethyl siloxane) (PDMS). After removal of the templating spheres by dissolution in toluene, porous polymer films were obtained, whose pore sizes depended on how much the original spheres had penetrated the substrate coating as a function of heating parameters. Thus, one sphere size could be used to obtain a relatively large range of pore sizes at the surface layer.

For porous membranes deposited electrochemically in a monolayer or bilayer of colloidal crystal spheres, the window diameters and shapes are controllable by the electrodeposition parameters.[81,82] Because electrodeposition fills the template from the bottom up, starting at the conducting substrate, the shape of interconnecting windows depends on the thickness of the deposited layer and on its relationship to the height of the template. With thin films less than 1/3 the diameter of the templating spheres, circular pores are formed. With film thicknesses close to the sphere diameter, pores with “irregular rounded triangular shapes” have been observed for galvanostatically electrodeposited CdSe films.[81] When the film thickness exceeds a monolayer, small vertical struts first grow between triangular holes in the template structure, subsequently forming complete cage structures and interconnected macropores as the film grows.[82]

4. Colloidal Crystals as Templates for Solids with Hierarchical Porosity

Through the use of multiple soft and hard templates, it is possible to create solids with multiple well-defined pore sizes.[29,83–85] Here, we will focus only on methods using colloidal crystals as one of the templates to create macropores. Smaller pores (small macropores, mesopores, or micropores) can exist within the solid wall skeleton. Such hierarchical porosity is beneficial in applications that require efficient mass transport through the interconnected macropore system, as well as high surface areas and size/shape selectivities of the smaller pores. Porosity within the wall may be present, even when a secondary template is not employed, resulting from textural mesoporosity between nanoparticles that make up the walls. In amorphous, sol–gel-derived walls, such as 3DOM silica, broadly distributed mesopores increase the specific surface area of the material, both in aqueous syntheses[66] and in syntheses employing supercritical CO_2.[86] In a recent preparation of 3DOM SiC from polymethylsilane, secondary mesopores were attributed to oxygen migration from the silica template to the framework, producing regions of silica in the framework that were washed out during HF treatment.[87]

However, the wall architecture can be better controlled when a secondary or even a tertiary template is employed, including ionic and nonionic surfactants, block copolymers, ionic liquids, structure-directing agents for zeolites, small colloids, and mixtures of these.[5,13,59,66,88–104] In these cases, the mesopore shapes and sizes become tunable, pore size distributions can be tightened, and surface areas can be controlled.

In syntheses of 3DOM silica with surfactant-templated mesoporous walls (3DOM/m silica), different mesostructures may be present, including disordered, wormlike structures, 2D-hexagonal channels, and cubic mesopore arrays.[103] However, due to confinement effects and different interactions between surfactant components and latex sphere surfaces, phase diagrams in colloidal-crystal-templated systems do not directly coincide with those for bulk systems. Furthermore, the orientation of mesochannels can differ in relation to the sphere (or macropore) surfaces. For example, in hierarchically structured silica monoliths, 2D-hexagonal channels are oriented perpendicular to the polymer spheres when the surfactant Brij 56 ($C_{16}H_{33}(OCH_2CH_2)_nOH$, $n \sim 10$) is used together with a cosurfactant, but they run parallel to the latex spheres when the polymeric surfactant P123 ($EO_{20}PO_{70}EO_{20}$) is employed (Figure 5). This orientation can affect the connection of adjacent macropores and mass transport through the pore systems. When multiple types of surfactants are used in one system (e.g., block copolymers and smaller surfactants), the complex interactions between them provide the means to influence the hierarchical structure, but they can also result in phase separation that may prevent hierarchical templating.[83]

Several recent syntheses have incorporated multiple sets of differently sized spheres as hard templates to produce hierarchical porosity.[13,105] Multilayered trimodal colloidal crystals were prepared by self-assembling 465-nm-diameter PS spheres, 84-nm-diameter PMMA spheres, and 6 nm silica

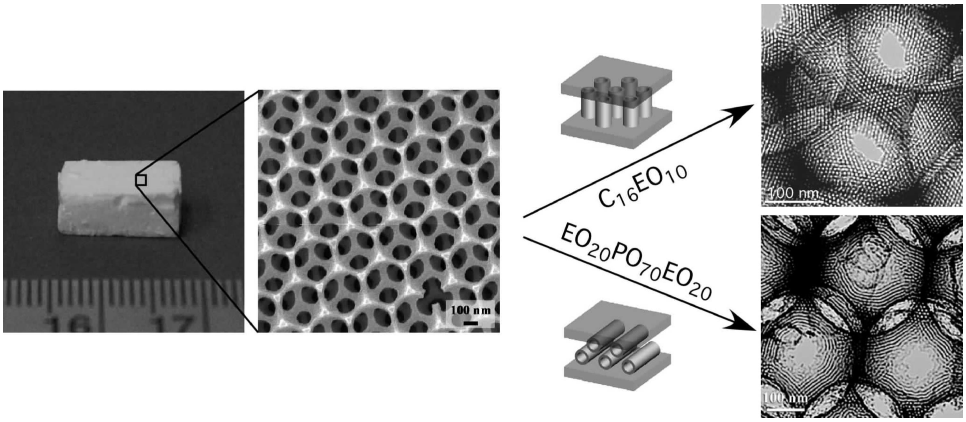

Figure 5. Photograph of a 3DOM/m silica monolith, SEM image showing the macropore structure, and TEM images of two different mesopore orientations. Reprinted with permission from ref 103, Li et al. *Langmuir* **2007**, *23*, 3996.

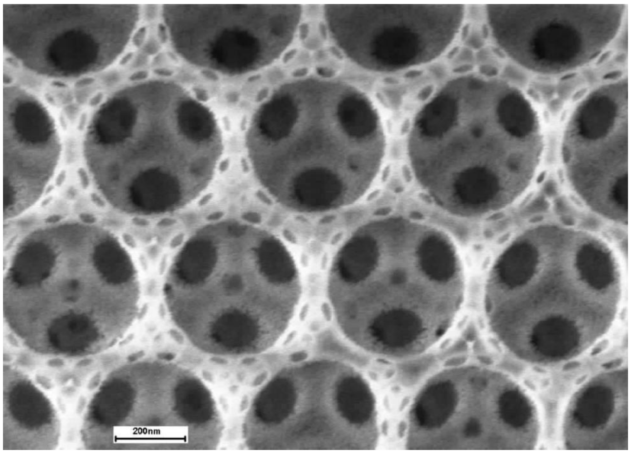

Figure 6. SEM image of silica with hierarchical pore structure prepared from multiple hard templates. Reprinted with permission from ref 13, Wang et al. *J. Am. Chem. Soc.* **2006**, *128*, 15606.

nanoparticles.[13] After calcination, these were converted to binary inverse opals, in which the silica walls around the larger macropores contained ordered voids templated by the PMMA spheres (see Figure 6).

3DOM/m carbon materials with both macropores and mesopores can be produced by nanocasting methods, in which 3DOM/m silica is infiltrated by carbonizable precursor materials, including sugars, furfuryl alcohol, pitch, aromatic molecules, acetonitrile, and phenol-formaldehyde precursors.[96,100] The resulting mesostructure is an inverse replica of the silica mesostructure, but at the macropore level, a 3DOM structure is directly replicated. In the case of vapor phase infiltration, the wall thickness and window sizes can be controlled through the infiltration time.[100] More direct syntheses of 3DOM/m carbon have recently been developed which circumvent the nanocasting step. One relies on triconstituent self-assembly of a surfactant template, carbon precursor, and silica precursor within a colloidal crystal template.[104] In a second method, hierarchically orderered macro-/mesoporous carbon was prepared by dual templating with a hard template (silica colloidal crystal) and a soft template (an amphiphilic triblock copolymer: $PEO_{127}-PPO_{70}-PEO_{127}$, Pluronic F127), using phenol-formaldehyde precursors dissolved in ethanol.[106] After carbonization and silica removal, quite large mesopores were obtained (ca. 11 nm diameter). The large mesopore sizes were ascribed to the ability of the silica template to prevent shrinkage of the mesostructure during thermosetting and carbonization. It was noted that annealing of the silica colloidal crystal at 100 °C was critical for obtaining hierarchically ordered porous carbon structures. Without such treatment, the macropore arrays were observed to collapse after impregnation and carbonization. In yet another method, the templating polymer spheres {poly[styrene-(co-2-hydroxyethyl methacrylate)]} acted as the source of carbon, depositing a carbon layer around smaller templating silica spheres during high-temperature pyrolysis in an inert gas.[105] After the removal of silica, the specific surface areas of the latter products (ca. 500–1000 $m^2\ g^{-1}$) were higher than in the absence of a secondary template but lower than those obtained with a soft secondary template.

Molecular imprinting, though not necessarily producing a secondary pore system, provides a way of templating 3DOM skeletal structures at a molecular length scale. A combination of colloidal crystal templating and molecular imprinting with L-dopa creates photonic crystal hydrogel films that detect the binding of specific enantiomeric analytes by changes in optical diffraction.[107] Here, the role of macropores is to shorten diffusion times and improve response times (ca. 20 s), as well as the capacity for analytes. Detection is based on L-dopa concentration-dependent fluorescence spectra. Interestingly, chiral regognition is detectable in this system even by eye.

5. Shaping Structures from the Nanoscale to the Bulk

5.1. Shaped Nano- and Microparticles. Having been formed by templates themselves, inverse opal structures lend themselves as suitable molds to create spherical nanoparticles with uniform, predetermined diameters. In this case, the inverse opal is infiltrated with precursors for the target spheres and removed to obtain the replica structure, often an interconnected array of solid spheres arranged in an opal structure. This “micromolding” or “lost-wax” approach has been used to synthesize spherical colloids of various oxides, sulfides, halides, carbides, metals, silicon, polymers, liquid crystals, and wax.[73,79,108–113] Polymeric inverse opals are convenient molds for this procedure, as they can be readily removed by calcination or dissolution. However, 3DOM silica, carbon, and soluble salt structures (3DOM NaCl and

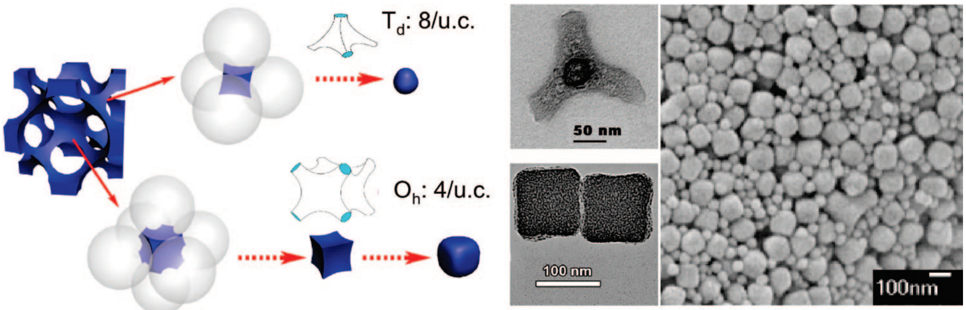

Figure 7. Shaped nanoparticles prepared by in situ disassembly of inverse opal skeletons. Reprinted with permission from ref 114, Li et al. *Angew. Chem. Int. Ed.* **2007**, *46*, 1885, copyright Wiley-VCH.

KCl) have also been employed as the micromolds. Nonspherical products, for example, ellipsoids, may be obtained by deformation of the template.[109] If interconnections between product particles are not too strong, discrete spheres can be isolated after ultrasonication of the sample. Otherwise, arrays of uniformly sized particles are produced. As in CCT, the interfacial chemistry plays an important role when an inverse opal is used as the template. For example, when inverse opal hydrogels with no acidic surface groups are used as molds for sol–gel titania, the sol–gel reaction proceeds in the macropores, and arrays of titania spheres are produced.[113] When the hydrogels are decorated with sulfonic acid or carboxylic acid surface groups, the sol–gel reaction occurs within the hydrogel walls instead, forming an interconnecting macroporous structure more typical of an inverse opal. Intermediate structures are observed at intermediate acid concentrations.

Quite a different approach to uniform nanoparticles shaped as cubes, tetrapods, or spheres is based on controlled in situ disassembly of the 3DOM skeleton (Figure 7).[114,115] Since this skeleton is templated by an *fcc* colloidal crystal, it is composed of bridged units whose shapes replicate octahedral and tetrahedral holes. Under conditions that weaken the bridges and place significant stress on them, the building blocks can separate into discrete particles during calcination of the sample. This is the case, for example, for dual-templated silica prepared from combined PMMA colloidal crystal and nonionic surfactant templates with TEOS as the silica source and oxalic acid as a catalyst for hydrolysis and condensation.[114] Under optimized conditions, the filled octahedral holes form cubic mesoporous silica particles whose edge lengths scale linearly with the diameters of the templating spheres. Filled tetrahedral holes have tetrapodal shapes, but these convert into spherical structures upon sintering. Because these particles form at calcination temperatures when most surface hydroxyl groups are lost, the shaped mesoporous silica particles do not aggregate strongly. This combined assembly/disassembly approach combines bottom-up syntheses (natural assembly of spheres, self-assembly of surfactants, and sol–gel reactions) with top-down methods (breaking apart structural elements) to produce nanoparticles with predetermined shapes and sizes. It has now been generalized to other systems, including carbon,[104,114] phosphated and nonphosphated titania and zirconia,[115] and several other shaped transition metal oxides.[116] Mesoporous polymer or carbon cubes and tetrapods were produced by nanocasting a polymer, using the shaped mesoporous silica particles as templates, and optionally carbonizing the polymer.[114] Mesoporous carbon cubes could also be generated more directly by self-disassembly of a concentrated triconstituent precursor solution (a soluble phenol-formaldehyde prepolymer, tetraethylorthosilicate, and the nonionic triblock copolymer F127) in a PMMA colloidal crystal.[104] At low concentrations of the triblock copolymer, monoliths with hierarchical porosity were obtained after pyrolysis in an inert atmosphere, but at higher concentrations, the structure disassembled into its uniform building blocks, which kept their shapes at temperatures as high as 1000 °C. The carbon−silica composite particles were converted either to mesoporous carbon particles by etching with hydrofluoric acid or to mesoporous silica particles by calcination in air. An even more direct synthesis of mesoporous carbon cubes eliminating the silica intermediate completely has recently been described.[117] In the synthesis of phosphated titania cubes, it was noted that the cubes self-assembled into close-packed three-dimensional arrays with simple cubic symmetry.[115,118] This surprising behavior was ascribed to combined effects of having a colloidal crystal template that predetermines the arrangement of cubes and including the low-melting phosphate phase, which can create capillary forces to bring cubes closer together. These templating methods will provide new opportunities to create extended 2D or 3D patterns and complex structures with novel architectures from the porous building blocks.

Whereas the formation of nanocubes in the above examples is dictated by the interstitial spaces in the template, nanocubes are also observed after pseudomorphic transformations of 3DOM silica to form macroporous $TiOF_2$ and TiO_2 products.[119] In this case, the cubic shape is not derived from the template but from the crystal structure of the first conversion product, $TiOF_2$, which is cubic. Notably, the cubic shape was preserved after a second conversion to anatase, which has a tetragonal crystal symmetry.

Shape is derived not only from individual macropores or building blocks within a unit cell; the morphology of materials prepared by CCT can also be influenced in larger dimensions. Confinement of colloidal crystals in emulsion droplets produces small, regularly structured clusters of microspheres whose shapes may be conferred to inverse replica structures. For example, dispersions of larger polystyrene microspheres and small silica or gold colloidal particles in water/toluene mixtures with an emulsion stabilizer

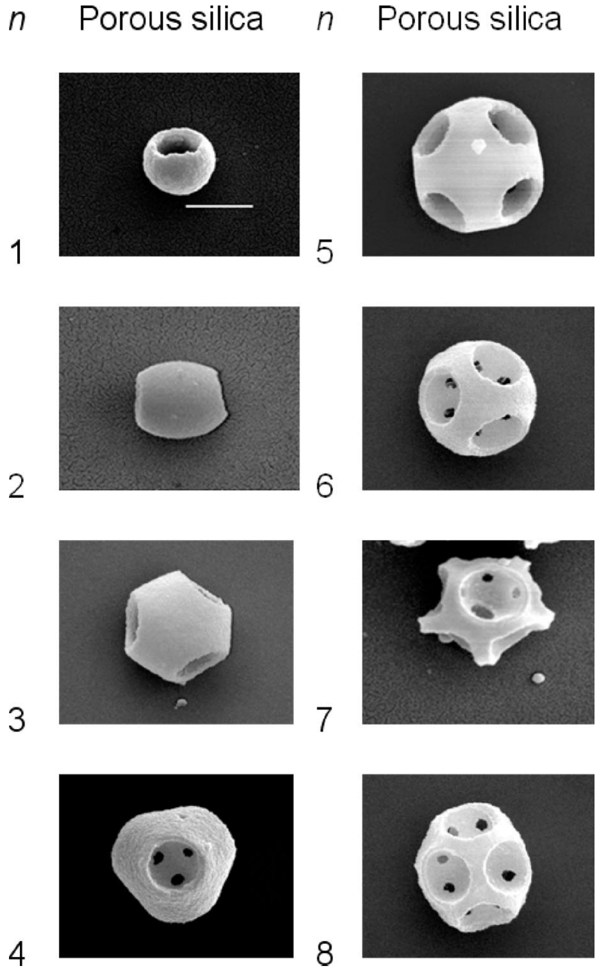

Figure 8. Scanning electron micrographs of porous silica particles prepared in emulsion droplets. The scale bar is 1 μm. Reprinted with permission from ref 120, Cho et al. *Chem. Mater.* **2007**, *19*, 3183.

spontaneously formed composite particles upon evaporation of toluene.[120] Elimination of the polymer spheres by calcination produced hollow silica (or gold) clusters with large well-coordinated windows (Figure 8). Similarly shaped porous titania particles were obtained by spray-drying mixed suspensions of brookite nanoparticles and polystyrene latex spheres.[121] Larger inverted silica photonic crystal balls with diameters of several tens of micrometers were templated from spherical colloidal particles that were self-organized within emulsion droplets by a microwave-assisted process.[122] It is possible to assemble colloidal crystal spheres in an emulsion first and subsequently infiltrate them with a wall precursor, a method that has been applied for the synthesis of titania photonic crystal balls.[123] These templating methods should also be applicable to semispherical clusters formed on a substrate, since a method for the reproducible preparation of sphere assemblies with controlled hemispherical shapes 10−100 μm in diameter has been described.[124] This process is based on drying microliter-sized sessile droplets containing colloidal spheres. The droplet shapes are manipulated by modifying the wetting behavior of the surface on which the droplets have been deposited.

5.2. Patterned 3DOM Structures. Line patterns of 3DOM structures are readily accessible using micromolding techniques.[125,126] For instance, patterned 3DOM carbon was prepared by ordering silica spheres within capillaries molded from PDMS, infiltrating them with phenolic resin, and carbonizing the material.[127] Similarly, hierarchically structured silica has been prepared by combining PDMS micromolding, polymer sphere templating, and the cooperative assembly of amphiphilic triblock copolymers with sol–gel precursors.[5] Patterns on conductive substrates are suitable for electrochemical deposition. As an example, 3DOM titania was electrochemically deposited inside a PS sphere template that was confined in a photoresist pattern on an indium tin oxide (ITO) substrate.[128] Even though colloidal spheres aggregated nonselectively over the whole substrate when they were grown by evaporation-assisted self-assembly, electrochemical growth of titania was confined to the patterned surfaces where ITO was exposed.

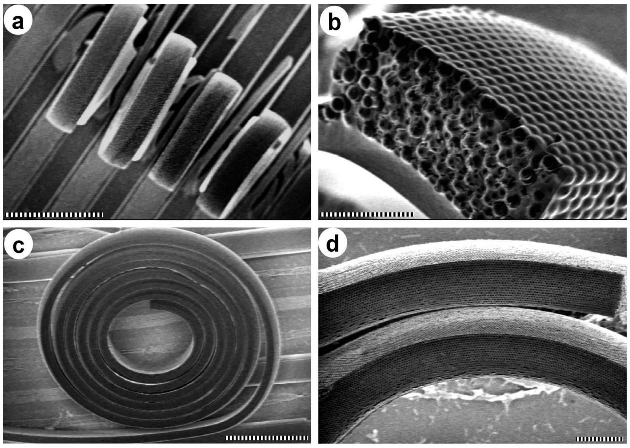

Figure 9. SEM images of curled zirconia inverse opal fibers. Reprinted with permission from ref 129, Vekris et al. *Adv. Mater.* **2006**, *18*, 2481, copyright Wiley-VCH.

In general, infiltration and drying conditions must be carefully controlled in order to maintain the integrity of the patterned 3DOM structure and to avoid cracks in the product. Differential shrinkage at regions where the film contacts the substrate or the mold can distort the templated structure. Such distortions can, however, be used to one's advantage, as was recently demonstrated for zirconia inverse opals. When zirconia inverse opal fibers are grown within a polymer relief pattern and capped with a denser overlayer, they sponteanously curl up upon release from the substrate if the hydrolysis of the precursors is carefully controlled during conversion to the oxide (Figure 9).[129] The curling effect is attributed to larger shrinkage in the overlayer than in the macroporous region. These curled fibers can be several millimeters in length and may be useful as curvilinear photonic crystal waveguides.

5.3. Larger 3D Shapes. While the pore symmetry in templated macroporous materials depends on the colloidal crystal template, the external shapes of templated crystalline inorganic materials can be dictated by the atomic crystal structure[130] and by the surface chemistry of the polymer template.[131] Requirements for single crystal growth throughout a template are that the equilibrium size of the crystal must be greater than the length scale of the template and the number of available nucleation sites must be small.[131] Calcite grown around a hydroxyl-functionalized polymer opal forms single crystals with rhombohedral morphology, and

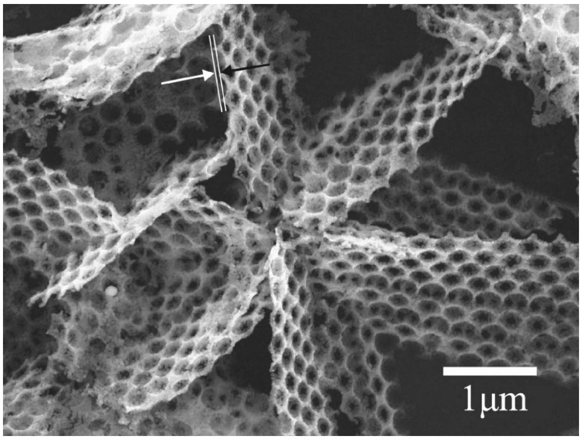

Figure 10. SEM image of porous ZnO nanosheets. Reprinted with permission from ref 134, Fu et al. *Adv. Mater.* **2006**, *18*, 1001, copyright Wiley-VCH.

cuprous oxide forms particles with octahedral morphology.[130] The particle morphology varies with the concentration of the functionalized latex spheres, which act as crystal growth modifiers. Although the spheres also play a templating role, they are only embedded in the surface layer. Even when latex particles are not assembled, they can be incorporated in zinc oxide crystals grown in the presence of graft polymers.[132] After solvent extraction or calcination, they produce a "Swiss cheese" morphology on the surface of the zinc oxide crystals. Zinc oxide grown by electrodeposition within a more ordered colloidal crystal thin film forms a porous wurtzite platelet structure.[133] The thickness of these porous nanosheets is dictated by the ZnO crystal sizes and not necessarily by the template. Even with multiple layers of spheres, it is possible to obtain much thinner nanosheets, down to a single grid layer (Figure 10).[134]

Although most preparations of 3DOM materials involve thin films or powders, structures with larger dimensions have been prepared, including wires and monoliths. For wires, opals can be grown and infiltrated inside capillaries, yielding cylindrical structures with high aspect ratios.[135] Porous metal wires were templated by electrodeposition within assembled spheres inside anodized alumina or polycarbonate membranes (Figure 11).[136] Free-standing, monolithic pieces of 3DOM materials (e.g., silica, carbon, and tungsten) several millimeters in each dimension have been grown from slowly sedimented colloidal crystal templates.[63,100,103,137–139] In these cases, capillary forces may be aided by positive or negative pressures to ensure thorough infiltration of the template.

6. Physical Properties of 3DOM Structures

6.1. Photonic Properties. Due to their regular 3D periodicity of low and high dielectric constant materials, inverse opals have been studied widely as photonic crystals, materials defined by spatial periodic variations in their dielectric functions. They comprise a class of materials in which electromagnetic interactions can be altered over certain wavelengths, which are typically close to the period of the structural modulation. Photonic crystals offer a range of potential applications, including low-threshold microlasers, ultrafast optical switches, microtransistors, antireflective coatings, sensors, and filters of electromagnetic radiation. Photonic crystals prepared by colloidal crystal templating have been reviewed recently,[140] and only a few selected studies will be used here to highlight structural effects on photonic properties.

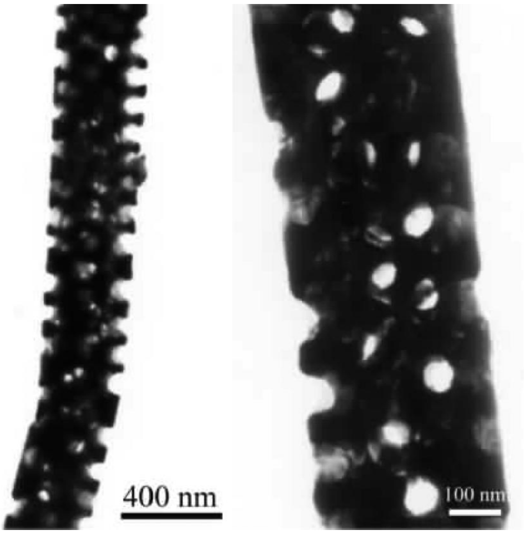

Figure 11. TEM images of porous Au wires templated inside membrane channels. Reprinted with permission from ref 136, Li et al. *J. Am. Chem. Soc.* **2003**, *125*, 16166.

When light undergoes coherent multiple scattering in these periodic structures, photonic bands are produced.[141] Depending on the scattering strength, light may not propagate in certain directions (stop bands) or in all directions (a full photonic band gap or PBG). These effects can lead to a localization of light within the photonic crystal structure, enhancement or inhibition of spontaneous emission, and modification of spontaneous emission rates. On the basis of theoretical calculations, the attainment of a full photonic band gap requires a high refractive index (RI) contrast, a large macropore content, and a very high degree of structural perfection in an *fcc* inverse opal.[56,141,142] The minimum RI contrast requirement for a full inverse opal is ~3.0, although it can be lowered to ~2.85 if the walls occupy less space than in an ideal inverse opal.[143] The photonic band structure depends critically on the shape and thickness of the skeletal walls. For example, calculations for silicon inverse opals with an egg-shell-like structure can possess a complete PBG between the eighth and ninth bands, whereas a cylindrical skeleton can have a second PBG between the fifth and sixth bands.[65,67,144]

Complete photonic bandgaps in the near-infrared range have been demonstrated for Si and Sb_2S_3 inverse opals.[145–147] In the case of Si, a PBG could be achieved in photonic crystals obtained from direct Si-CVD infiltration of silica opals[145] and in photonic crystals prepared by Si deposition in preformed inverse silica opal micromolds.[73] When amorphous Si walls in these materials were converted to polycrystalline walls, the nonlinear optical response of the photonic crystals was modified from an absorptive response to a mainly dispersive response.[148] This nonlinear response is of interest in the context of ultrafast optical switching. Among oxide photonic crystals, titania has received special attention because of the relatively high refractive index and optical transparency of this wide bandgap semiconductor in the visible range.[3,4,58,65–67,71] With an RI contrast of 2.5 for 3DOM anatase (the phase more readily synthesized with a well-ordered macropores structure), a complete PBG is not yet produced, but stop bands in the visible or UV regions overlap for a wide range of angles covering over 55% of all directions.[3,71,149]

When light sources, such as dye molecules, rare earth ions, and semiconductor nanoparticles, are embedded in inverse opal photonic crystals, the spontaneous emission of light originating from these sources can be strongly modified.[150–155] Alternatively, the 3DOM skeleton may act as a light source whose emission is affected by its periodic structure.[43,156–159] Depending on the position of the light source within the unit cell, stop-band positions, intensities, widths, and emission lifetimes may be altered in an angle-dependent manner.[155,160] These properties allow one to tune the emission spectrum, directionality of emission, and the rate of emission.

The unique photonic crystal properties have been exploited in a number of photocatalytic systems. An elegant approach to enhancing the photoactivity of titania involves the use of the 3DOM structure to increase the path length of light within this catalyst. The photonic crystal structure reduces the group velocity of light near the edges of the photonic stop band. If the photon energy overlaps with the absorbance of titania, enhanced absorption is expected.[161] Titania photonic crystals have been considered as components in dye-sensitized photoelectrochemical cells designed to increase the efficiency of the solar cells.[162–166] In these applications, the inverse opal architecture can improve the efficiency of the solar cells in various ways related to structural and optical properties of the photonic crystal. The continuous void structure permits a thorough penetration of dyes and other cell components throughout the material.[164] A large interfacial area ensures good contact between the dye and the semiconductor walls. Multiple backscattering at disordered regions and interfaces between porous titania and nanocrystalline titania, together with Bragg diffraction effects and a localization of heavy photons near the edges of photonic gaps, can enhance photocurrent efficiencies significantly.[162,163,166] The relative effects of ordered and disordered regions in macroporous titania on the efficiency of photoelectrochemical cells are still under discussion. Within a given 3DOM titania film, the photocurrent increased by a factor of 10 when the illuminating beam was focused on a low-defect spot of the film rather than being averaged over the whole film area which contained cracks and other defects.[165] In contrast, intentionally disordered macroporous titania films prepared by templating with spheres of mixed sizes showed better photoelectrical performance than more ordered inverse opal films.[166]

Another application of inverse titania opals, namely, the photocatalytic degradation of organic molecules, also displayed a relatively high tolerance for structural defects in the photonic crystal.[161] With a suitable overlap of irradiating light and the long-wavelength edge of the photonic stop band, the degradation rate of a solid organic dye deposited on the photonic crystal walls was doubled for well-ordered materials (compared to nontemplated nanocrystalline titania), and even with defect concentrations up to 40%, the photodegradation rate was enhanced by ca. 50%.[167] This behavior implies the feasibility of applying titania inverse opals for environmental remediation, even if the structure is not completely perfect.

A different structured semiconductor, 3DOM Cu_2O prepared by electrodeposition, was shown to display higher photocurrent efficiencies than nonstructured bulk Cu_2O and to speed up the photoelectroreduction of oxygen under visible light illumination.[168] The improved performance in the 3DOM material was attributed to greater light absorption and decreased recombination of the charge carriers as a result of the thin walls and short diffusion paths between the location of charge carrier generation and the interface between the semiconductor and the electrolyte.

With certain exceptions, such as the one mentioned above, structural perfection is extremely important for dielectric photonic crystals.[169–172] Potential defects in inverse opal structures include defects inherited from the template, shrinkage-induced cracks, point defects from wall breakage, and misaligned domains. A useful method has now been developed to map out the crystalline quality and the period of photonic crystals by laser diffraction.[173] Domains of 25–500 μm^2 separated by cracks were mapped in thin film inverse opal WO_3 structures templated from 890-nm-diameter PS spheres. In relatively large regions (up to 0.4×0.4 mm^2), domains had the same crystallographic orientation, despite cracks between domains. This method can be used as long as the laser wavelength is less than the photonic crystal lattice period and is therefore most applicable for photonic crystals designed for the infrared regime. To avoid crack formation in the first place, composites of active material (e.g., preformed Ge nanoparticles) with a photocuring adhesive have been employed for infiltration of a colloidal crystal template.[174] While the crack density was indeed reduced in this low-temperature synthesis, dilution of the semiconductor nanoparticles with the photoadhesive lowered the effective refractive index of the photonic crystal.

The introduction of engineered defects into 3DOM structures can promote the propagation and collection of light within the photonic crystals. Random positioning of point defects occurs by doping the colloidal crystal template with a small fraction of differently sized spheres.[146] More controlled defect placement is possible, for example, by sequential deposition of silica and polystyrene spheres to incorporate 2D planar defects into the colloidal crystal template (Figure 12, left),[175] or by writing 3D defect structures into photosensitive polymer photonic crystals using multiphoton polymerization and confocal imaging.[176] A recent example of this process demonstrated a direct writing of 3D defects within a mechanically stable, transparent 3DOM ORMOCER photonic crystal.[177,178] The photonic crystal was infiltrated with a photosensitive resin that had a similar refractive index as the photonic crystal. This resin was photopolymerized in desired regions by two-photon lithography. Unexposed regions were removed, leaving the designed defects in the structure (Figure 12, right). If fluorescing species were included in the resin, fluorescent defects could be produced in the photonic crystal with the

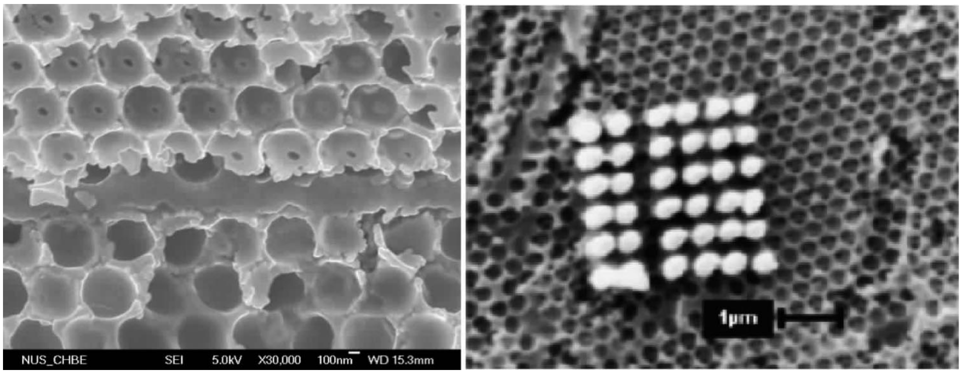

Figure 12. Left: SEM image of an inverted opal with a planar defect. Reprinted with permission from ref 175, Wang et al. *Langmuir* **2006**, *22*, 1369. Right: SEM image of defects introduced on the surface of an ORMOCER inverse opal using two-photon lithography. Reprinted with permission from ref 178, Lange et al. *Macromol. Rapid Commun.* **2007**, *28*, 922, copyright Wiley-VCH.

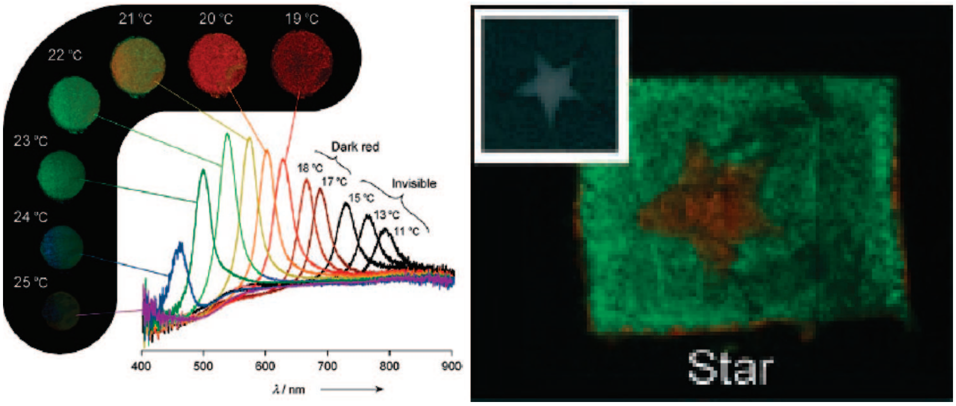

Figure 13. Photographs and reflection spectra of a porous hydrogel at various temperatures. This hydrogel contained photoresponse azobenzene groups that undergo dipole moment changes upon photoisomerization, producing a structural color change by irradiation with UV light through a photomask. Reprinted with permission from ref 185, Matsubara et al. *Angew. Chem., Int. Ed.* **2007**, *46*, 1688, copyright Wiley-VCH.

spatial resolution of the two-photon source. In these techniques, it is critical to match the refractive index between the photonic crystal and the resin closely to avoid light scattering.

While the optical properties of photonic crystals can be tuned statically through structural design by methods described earlier, dynamic control is important for applications involving switching, sensing, and display. Tuning of optical properties was demonstrated for ferroelectric and electrochromic inverse opals. In ferroelectric (Pb,La)(Zr,Ti)O_3 inverse opals, optical stop bands shifted continuously and reversibly over a small wavelength range with the application of an electric field as the RI varied via an electro-optic effect.[179] In electrochromic 3DOM WO_3, Li intercalation into the crystals caused reflection peak shifts as a function of applied voltage.[180] Another way to build in a dynamic response is to allow the pore spacing to change as a function of environmental stimuli. This has been demonstrated, for example, in the case of hydrogels that undergo large and often reversible volume changes as a function of temperature, humidity, pH, ionic strength, solvent composition, and the presence of specific analytes.[181–185] Such volume changes alter the unit cell dimensions of the photonic crystal and therefore the positions of optical stop bands (Figure 13). Because the open inverse opal structure allows a rapid influx or release of water, swelling or shrinking can be more than 1000 times faster than in conventional homogeneous gels.[185] In supported hydrogels, the structural changes depend on pinning of the hydrogel to the substrate. A detailed investigation of structural changes in a fluorescently labeled, hydrogel-based inverse opal thin film as a function of swelling revealed that diffraction responses rely on changes in the interlayer distance perpendicular to the substrate.[186] Stress or pressure applied on deformable inverse opal films also results in local changes of stop-band position, reflection intensity, and peak widths, an effect which may be utilized for biometric recognition and real-time, mechanical sensing.[187–189]

Dynamic tunability of optical band structures is also possible by changing the effective refractive index of the void spaces in inverse opals through the choice of fillers. Stop-band positions shift when the pores are infiltrated with liquids of various refractive indices.[2] Such responses can be monitored in situ using flow cell arrangements.[190] With liquid crystal fillers, optical properties change in response to electric fields, photoinduced transitions, or both.[191–196] As an interesting alternative to infiltration with liquid crystals, a double-inverse-opal photonic crystal (DIOPC) was recently prepared by assembling a colloidal crystal from core–shell structures with a silica sphere core and a polymer skin.[197] This was infiltrated with TiO_2 by CVD methods. Upon low-temperature calcination, the PMMA component was removed, yielding 3DOM TiO_2 in which the macropores contained silica spheres and forming a 3D array of "rattles." With randomly filled pores, the 3DOM titania−silica sphere

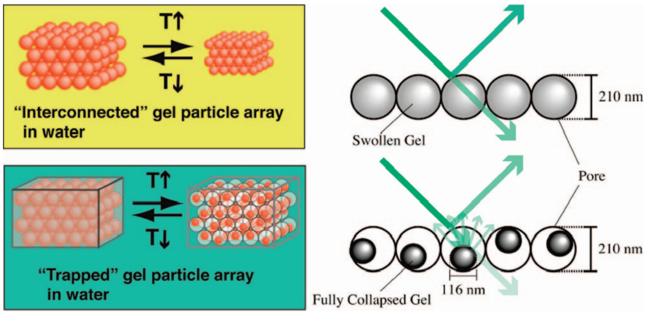

Figure 14. Left: Schematic showing the responses of “interconnected” gel particle arrays and “trapped” gel particle arrays, both immersed in water, to changes in temperature. Right: Schematic illustrating the difference in light scattering for the two gel particle arrays. Reprinted with permission from ref 198, Kumoda et al. *Langmuir* **2006**, *22*, 4403.

DIOPC scattered light diffusively. When the material was filled with a fluid that matched the refractive index of silica, a distinct stop band was observed. With uniform pore filling and a higher refractive index contrast, photonic bandgap switching, perhaps by electric or magnetic fields, should be possible for this interesting geometry.

A similar structure was prepared by trapping a hydrogel inside a 3DOM PS membrane and exposing this array to ethanol.[198] The product, when immersed in water, responded to changes in temperature very differently compared to an interconnected array of hydrogel spheres that was not trapped in a polymer membrane. The interconnected gel particles showed reversible changes in spectral peak positions with temperature as the hydrogel shrunk or swelled. On the other hand, the trapped gel particles in the more robust porous polymer membrane produced large, reversible peak intensity changes with temperature, but the peak positions did not change because the unit cell of the photonic crystal was fixed by the PS matrix. The change in peak intensity is associated with enhanced light scattering when the gel spheres shrink and do not fill macropores completely (Figure 14).

6.2. Magnetic Properties and Superconductivity. Unusual magnetic properties of 3DOM materials were first noted for 3DOM Co composed of 3–4 nm Co grains surrounded by a CoO surface layer.[199] Shifts in hysteresis loops of magnetic moment versus magnetic field measurements were associated with exchange bias, resulting from the antiferromagnetic CoO skin. A nonmonotonic temperature dependence of the coercivity was related to the spin-glass-like state of the Co nanoparticles below a critical temperature. Additional studies of inverse opals composed of Ni, Fe, and their alloys demonstrated significant coercivity saturation field enhancements of the porous metals compared to denser films.[110,200–203] The coercivity and saturation fields increase as pore sizes and wall dimensions decrease. For pore sizes below 200 nm, the coercivity decreases again. The peak in the coercivity occurs at dimensions where magnetization switches from multidomain to single-domain behavior.[203] The 3DOM skeleton pins individual nanoparticle domains together, leading to structure-dependent coercivities.[202,203] Other magnetic inverse opals that have been prepared include the pyrolysis product of 3DOM polyferrocenylsilane, which contains ferromagnetic γ-Fe_2O_3 particles[204] and the magnetic oxide, 3DOM $La_{0.7}Ca_{0.3-x}Sr_xMnO_3$.[35] In the latter material, a temperature-independent, large negative magnetoresistance was attributed to spin-polarized tunneling at grain boundaries between nanoparticles. Superconductivity is also modified as a function of the wall confinement introduced by a colloidal crystal template. In lead inverse opals, a very slight increase in superconducting temperature compared to bulk lead was measured, but the upper critical field increased by a factor of 4.[62] The superconductivity was particle-size-dependent, again pointing to the importance of accurate control over the wall structure.

6.3. Wettability. Several recent experiments have demonstrated significant control over the wetting behavior of templated surfaces via their architecture and surface composition.[205–208] 3DOM structures possess a high degree of surface roughness, which can result in either strong hydrophilic or superhydrophobic interactions, depending on functional groups present at the surface. One can take advantage of these effects to prepare surfaces with statically tunable or dynamically switchable wetting behavior. For example, inverse opal silica monolayers display hydrophilic behavior, producing a water contact angle of 5° compared to 10° on flat silica films.[206] After surface modification with a fluoroalkylsilane, the film becomes superhydrophobic, with a water contact angle of up to 155°, that is, 40–55° higher than for a flat fluoroalkylated film.[205] In spite of the superhydrophobic behavior, small water droplets remain firmly pinned to the surface, even when the films are turned upside down.[206] A further increase in contact angle to 165° is effected by distorting the pore structure through deformation of the PS template with heat. Sintering the template changes the contact of the silica network from a pointed to a more faceted shape. In addition to the resulting increase in hydrophobicity, the structural modification also increases the mobility of water droplets. In the case of macroporous polyvinylidine fluoride films, a water contact angle up to 153° has been achieved, depending on the filling fraction of the polymer and diameters of templating silica spheres.[207] This compares to an angle of 106° for smooth polyvinylidine fluoride films. By introducing photoswitchable surface groups to an inverse opal film, the surface wettability of the film can be dynamically and reversibly controlled by an external light source.[208] 3DOM silica films were modified by the electrostatic layer-by-layer self-assembly of cationic and anionic polyelectrolytes with azobenzene side groups. Azobenzene groups undergo transitions from the trans to the cis form upon irradiation with UV light and revert to the original state after exposure to visible light. Due to differences in dipole moment between the two states, the surface free energy also varies, and as a result, the water contact angle is modified. Surfaces with switchable wettability are of interest, for example, for microfluidic switching, antifogging, and self-cleaning surfaces.

7. Integrating 3DOM Structures in More Complex Assemblies

While several proposed applications of 3DOM materials benefit from their structure directly, others require that additional components be incorporated either within or outside of the macroporous material. In addition to the

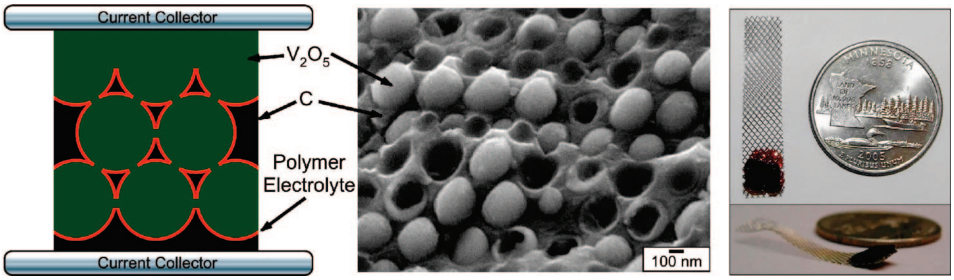

Figure 15. Left: Schematic diagram of a 3D nanostructured interpenetrating electrochemical cell. Macropores in 3DOM carbon were coated with a poly(phenylene oxide) layer and infiltrated with vanadia. After lithiation, this cell was charged to 3.2 V and was electrochemically cycled. Middle: SEM image of the cycled cell. Right: Photograph of the 3DOM carbon electrode mounted on a metal mesh current collector. Reprinted with permission from ref 44, Ergang et al. *Adv. Mater.* **2006**, *18*, 1750, copyright Wiley-VCH.

complex photonic crystal structures highlighted in section 6.1, a few relatively complex assemblies of coatings, nanoparticles, clusters, and other structures have recently been built around inverse opals to demonstrate applications in electrochemistry, sensing, and catalysis.

One example involves electrodes with interconnected macroporous structures. A range of porous metallic, oxide, and semiconductor electrodes have been prepared by colloidal crystal templating for applications including lithium ion batteries, fuel cells, electrochemical double-layer capacitors, sensors, and electrocatalysts.[40,138,209–222] The advantages of the open, interconnected pore architecture for electrodes are multifold. The bicontinuous structure permits the conduction of ions or electrons throughout the skeleton while also providing a continuous path in the pore system that can allow complete penetration of the electrolytes, active phases, and guest molecules. Nanostructured dimensions keep diffusion pathlengths through the walls relatively short. Surface areas are larger than in planar electrodes, in some cases, much larger. As a result of these structural advantages, electrodes for lithium insertion/deinsertion display greater capacities at high rates than similarly prepared, nontemplated electrodes, as long as volume changes in the 3DOM skeleton during lithium exchange can be avoided.[40,209,211,217,218]

Importantly, for the construction of complex assemblies, the macropores provide sufficient room for other components. For example, a 3D interpenetrating electrochemical cell was recently assembled by coating a monolithic 3DOM carbon electrode with an ultrathin layer of poly(phenylene oxide) which electronically separated the carbon from a vanadia cathode phase that was subsequently added to the pores (Figure 15).[44] In spite of submicrometer component dimensions, the cell could be reversibly charged and discharged, although its performance was still limited by the low electronic conductivity of the cathode structure. Monolithic 3DOM carbon electrodes also formed the basis for an ultrastable ion-selective electrode with good resistance to interference from oxygen and light.[223] Here, the carbon provided a stable solid contact between an ionophore-doped solvent polymeric membrane and an external metal contact (Figure 16). The 3DOM carbon interlayer was capable of both ionic and electronic charge transfer.

For use as proton conductive membranes in fuel cells, 3DOM materials may, in the future, provide an alternative to relatively expensive Nafion membranes. Sulfonation of 3DOM silica enhances proton conductivity by a factor of 400.[224] This material was incorporated in a proton-conducting gel polymer to form a composite membrane that also exhibited high proton conductivity. A self-supporting 3DOM polyimide membrane infiltrated with a proton conductive gel polymer electrolyte exhibited a proton conductivity of 1.2 × 10^{-1} S cm^{-1} at 60 °C, comparable to that of Nafion membranes, but smaller than expected for the infiltrated gel polymer electrolyte.[225] The difference was attributed to the isolation of a fraction of pores that lacked interconnecting windows. Even though the 3 × 3 cm^2 membrane was only 200-μm-thick, it was mechanically stable.

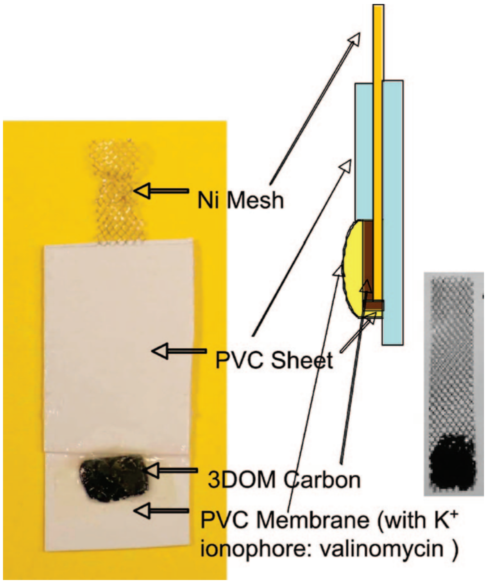

Figure 16. Photograph and schematic of 3DOM carbon-contacted ion-selective electrode. The photograph on the right shows the uncovered Ni-mesh/3DOM carbon contact.[223]

The void space in 3DOM electrodes is large enough to immobilize redox-active proteins and enzymes that are active in sensing, in conversion, and as biofuel cells. In an electrodeposited 3DOM gold film, direct electron transfer was possible between adsorbed hemoglobin and the electrode.[226] As a result of the high surface area of the macroporous structure, the surface density of attached hemoglobin groups was significantly increased compared to planar gold electrodes. A similar advantage was found for the electroenzymatic oxidation of glucose on shaped 3DOM gold ultramicroelectrodes, where the oxidation current was enhanced by an order of magnitude compared to a nonporous electrode.[227,228] Here, it was important that the target enzyme was able to diffuse through interconnected macropores to make use of the whole surface area. The activity tends to be higher than on planar electrodes for slow redox reactions, but not for redox reactions with fast kinetics, which occur mainly on the outermost pore layer before ions can diffuse into the lower lying pores. An electrochemical response similar to that of flat graphite electrodes was also noted for graphitic 3DOM carbon films in cyclic voltammmetry experiments with ferrocene, suggesting that only the outer surface of the carbon film was electrochemically active.[222]

An interesting example of optical sensing based on an integrated 3DOM structure is based on a transparent inverted opal hydrogel with large pores (several tens of micrometers), modified with a fluorescent layer of tris(4,7-diphenyl-1,10-phenanthroline) ruthenium chloride ($Ru(dpp)_3$).[229] The pores are large enough to accommodate human bone marrow cells, and the pore interconnectivity ensures a rapid diffusion of liquids and oxygen into the scaffold, giving a response time on the order of minutes. Because the emission of $Ru(dpp)_3$ is quenched by oxygen, the emission intensity is stronger in cell-rich areas where oxygen levels are reduced by oxygen consumption of the cells. Although measurements were not yet quantitative, this sensor design may in the future permit the 3D mapping of oxygen levels during cell growth using confocal microscopy.

Because of their high thermal stabilities, chemical inertness, and ability to disperse active catalysts over a relatively high surface area, 3DOM ceramics have been integrated in patterned microreactor systems. For example, macroporous SiC was patterned in a PDMS mold on a SiO_2/Si substrate by a micromolding technique.[230] The preceramic precursors were pyrolyzed around polymer or silica spheres, then loaded with ruthenium to demonstrate the high temperature decomposition of NH_3 to produce hydrogen for polymer electrolyte membrane fuel cells. The next version of these reactors enclosed the inverse opal SiC monoliths within high-density alumina reactor housings.[231] This system enabled high turnover frequencies, and the pressure drop was 2 orders of magnitude lower than in packed beaded structures with the same geometric surface area. The same advantage of low pressure drops was also reported for Al_2O_3 inverse opals,[70] loaded with a MoO_3-promoted Pt catalyst and encased in a stainless-steel microchannel reactor (Figure 17).[232] This catalyst system permitted the complete conversion of propane at a temperature as low as 300 °C.

8. Summary and Outlook

After a decade of research on colloidal crystal templating, the macroporous products have reached a new level of sophistication. It is now possible to direct the shape and thickness of the walls in 3DOM materials in addition to their internal textures. Pore sizes can be tuned statically or dynamically. External morphologies are shapeable, and patterns can be formed. Complex assemblies of different compositions have been prepared within the confinement of voids. Structural defects have been reduced to some extent, and various methods to introduce intentional defects in photonic crystal structures have been described. As a result of structural tunability, physical and reactive properties of inverse opals can be modified to benefit a wide range of applications. In addition, 3DOM structures have been employed to generate porous and nonporous nanoparticles of defined sizes and shapes, providing exciting new opportunities to study basic properties of shaped nanoparticles and adding to the choice of building blocks for nanoparticle assemblies.

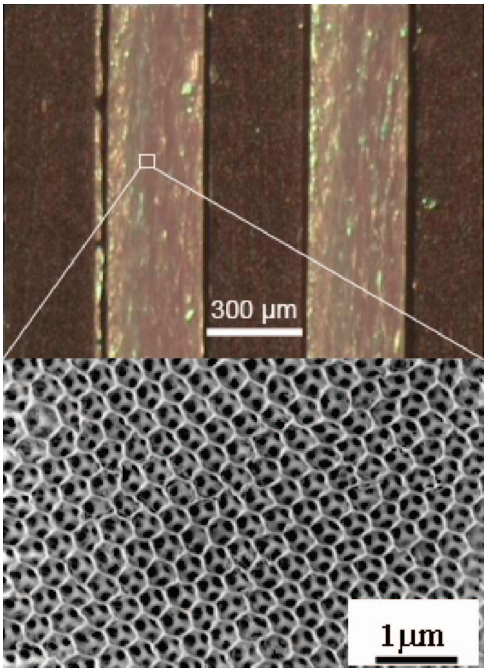

Figure 17. Top: optical micrograph of Al_2O_3 inverse opals in microchannels. Bottom: SEM image of the inverse opal. Reprinted with permission from ref 232, Guan et al. *Chem. Commun.* **2007**, 260, copyright Royal Society of Chemistry.

As our ability to manipulate the infiltration and skeleton-forming steps increases, the template itself will require further attention. One aspect of structural control by colloidal crystal templating that is still lagging is the symmetry of the product. A few colloidal crystal templates with non-*fcc* symmetry have been described, and these are amenable to infiltration to produce inverse replica structures.[22–24,233–238] However, over large length scales (including the third dimension), methods of achieving such structures remain too complex to be applied as broadly as *fcc* structures. If alternate methods are employed to achieve lower-symmetry structures, including methods using holographically prepared templates or templates made from "writing methods" (dip-pen lithography, direct laser writing, and traditional lithographic methods), these techniques can also profit from the wealth of knowledge gained from the development of CCT techniques, including an understanding of template−precursor interactions, growth in confinement, and structural changes during the processing of very open nanostructured solids.

Another issue that should be addressed as application development becomes more mature is scaleup. The current bottleneck relates largely to the colloidal crystal template. Many investigators have employed small areas of thin opaline films as templates. This may be, in part, a matter of convenience for the desired measurements, but it is also an issue of cost. Commercial colloids of sufficient uniformity to produce high-quality colloidal crystals remain expensive, especially if the desired diameters fall outside a limited range (approximately 0.1–1 μm). In certain applications, cheaper alternate porogens (e.g., emulsion droplets) can provide the desired porosity in templated materials. However, such porogens do not guarantee the periodicity needed in optical applications or the interconnectedness of pores required where periodicity may not matter as much as mass transport through the pores. Hence, it will be necessary to develop inexpensive, scaleable methods of preparing suitable template particles with controllable surface properties, softening temperatures, solubilities, and especially narrow size dispersity. Larger-scale 3DOM film and monolith preparations should then be possible by coating and batch techniques, respectively.

On the basis of a survey of the current literature, colloidal crystal templating has now caught the attention of several distinct disciplines, with each recognizing diverse advantages of the templated porous products. This multidisciplinary interest in 3DOM architectures has led to rapid developments in this area, and it provides a strong basis for continued progress in the future. Already, several proofs of concept have been provided that demonstrate advantages of 3DOM architectures in applications as varied as photonics, sensing, fuel cells, and photocatalysis. In the next few years, one can expect an integration of materials prepared by CCT into other complex systems that may utilize multiple functions of these nanostructured porous materials. The degree of structural and compositional control in the templated structures will increase even further. Significant advances in templating methods combined with guidance from continually improving band structure calculations will likely facilitate bottom-up syntheses of photonic crystals with full photonic bands in the visible region. And inverse opals will continue to sparkle.

Acknowledgment. The preparation of this review was financially supported by the Petroleum Research Foundation, administered by the American Chemical Society (ACS-PRF grant number 42751-AC10), the U.S. Department of Energy (DE-FG02-06ER46348), the Office of Naval Research (grant number N00014-07-1-0608), and by the National Science Foundation (DMR-0704312).

References

(1) Blanford, C. F.; Yan, H.; Schroden, R. C.; Al-Daous, M.; Stein, A. *Adv. Mater.* **2001**, *13*, 401–407.
(2) Schroden, R. C.; Al-Daous, M.; Blanford, C. F.; Stein, A. *Chem. Mater.* **2002**, *14*, 3305–3315.
(3) Wijnhoven, J. E. G. J.; Vos, W. L. *Science* **1998**, *281*, 802–804.
(4) Holland, B. T.; Blanford, C. F.; Stein, A. *Science* **1998**, *281*, 538–540.
(5) Yang, P.; Deng, T.; Zhao, D.; Feng, P.; Pine, D.; Chmelka, B. F.; Whitesides, G. M.; Stucky, G. D. *Science* **1998**, *282*, 2244–2246.
(6) Blanford, C. F.; Carter, C. B.; Stein, A. *J. Microsc. (Oxford, U.K.)* **2004**, *216*, 263–287.
(7) Velev, O. D.; Jede, T. A.; Lobo, R. F.; Lenhoff, A. M. *Nature* **1997**, *389*, 447–448.
(8) Zakhidov, A. A.; Baughman, R. H.; Iqbal, Z.; Cui, C.; Khayrullin, I.; Dantas, S. O.; Marti, J.; Ralchenko, V. G. *Science* **1998**, *282*, 897–901.
(9) Park, S. H.; Xia, Y. *Chem. Mater.* **1998**, *10*, 1745–1747.
(10) Gierszal, K. P.; Yoon, S. B.; Yu, J.-S.; Jaroniec, M. *J. Mater. Chem.* **2006**, *16*, 2819–2823.
(11) Huang, L.; Wang, Z.; Sun, J.; Miao, L.; Li, Q.; Yan, Y.; Zhao, D. *J. Am. Chem. Soc.* **2000**, *122*, 3530–3531.
(12) Wang, Y. J.; Tang, Y.; Ni, Z.; Hua, W. M.; Yang, W. L.; Wang, X. D.; Tao, W. C.; Gao, Z. *Chem. Lett.* **2000**, *510*, 511.
(13) Wang, J.; Li, Q.; Knoll, W.; Jonas, U. *J. Am. Chem. Soc.* **2006**, *128*, 15606–15607.
(14) Caruso, F.; Caruso, R. A.; Möhwald, H. *Science* **1998**, *282*, 1111–1114.
(15) Dong, A.; Wang, Y.; Tang, Y.; Zhang, Y.; Ran, N.; Gao, Z. *Adv. Mater.* **2002**, *14*, 1506–1510.
(16) Hotta, Y.; Jia, Y.; Kawamura, M.; Omura, N.; Tsunekawa, K.; Sato, K.; Watari, K. *J. Mater. Sci.* **2006**, *41*, 2779–2786.
(17) Dinsmore, A. D.; Crocker, J. C.; Yodh, A. G. *Curr. Opin. Colloid Interface Sci.* **1998**, *3*, 5–11.
(18) Xia, Y.; Gates, B.; Yin, Y.; Lu, Y. *Adv. Mater.* **2000**, *12*, 693–713, and references therein.
(19) Colvin, V. L. *MRS Bull.* **2001**, *26*, 637–641.
(20) Texter, J. *C. R. Chim.* **2003**, *6*, 1425–1433.
(21) Wong, S.; Kitaev, V.; Ozin, G. A. *J. Am. Chem. Soc.* **2003**, *125*, 15589–15598.
(22) Wang, D.; Moehwald, H. *J. Mater. Chem.* **2004**, *14*, 459–468.
(23) Dziomkina, N. V.; Vancso, G. J. *Soft Matter* **2005**, *1*, 265–279.
(24) McLellan, J.; Lu, Y.; Jiang, X.; Xia, Y. Self-assembly of colloidal building blocks into complex and controllable structures. In *Nanoscale Assembly*; Huck, W. T. S., Ed.; Springer: New York, 2005; pp 187–216.
(25) Stein, A. *Microporous Mesoporous Mater.* **2001**, *44–45*, 227–239.
(26) Stein, A.; Schroden, R. C. *Curr. Opin. Solid State Mater. Sci.* **2001**, *5*, 553–564.
(27) Norris, D. J.; Vlasov, Y. A. *Adv. Mater.* **2001**, *13*, 371–376.
(28) Meseguer, F.; Blanco, A.; Miguez, H.; Garcia-Santamaria, F.; Ibisate, M.; Lopez, C. *Colloids Surf., A* **2002**, *202*, 281–290.
(29) Stein, A.; Schroden, R. C. Designing Porous Solids Over Multiple Pore Size Regimes. In *Nanostructure Science and Technology*; Jones, C. W., Scott, S. L., Crudden, C. M., Eds.; Kluwer Plenum: Dordrecht, The Netherlands, 2002; Vol. 3, pp 257–276.
(30) Xia, Y.; Lu, Y.; Kamata, K.; Gates, B.; Yin, Y. Macroporous materials containing three-dimensionally periodic structures. In *Chemistry of Nanostructured Materials*; Yang, P., Ed.; World Scientific: Singapore, 2003; pp 69–100.
(31) Schroden, R. C.; Stein, A. 3D ordered macroporous materials. In *Colloids and Colloid Assemblies*; Caruso, F., Ed.; Wiley-VCH: Weinheim, Germany, 2004; pp 465–493.
(32) Lytle, J. C.; Stein, A. Recent Progress in Syntheses and Applications of Inverse Opals and Related Macroporous Materials Prepared by Colloidal Crystal Templating. In *Annual Reviews of Nano Research*; Cao, G., Brinker, C. J., Eds.; World Scientific Publishing Co.: River Edge, NJ, 2006; Vol. 1, pp 1–79 and references therein.
(33) Geraud, E.; Prevot, V.; Ghanbaja, J.; Leroux, F. *Chem. Mater.* **2006**, *18*, 238–240.
(34) Chen, F.; Xia, C.; Liu, M. *Chem. Lett.* **2001**, *30*, 1032–1033.
(35) Kim, Y. N.; Kim, S. J.; Lee, E. K.; Chi, E. O.; Hur, N. H.; Hong, C. S. *J. Mater. Chem.* **2004**, *14*, 1774–1777.
(36) Sadakane, M.; Takahashi, C.; Kato, N.; Ogihara, H.; Nodasaka, Y.; Doi, Y.; Hinatsu, Y.; Ueda, W. *Bull. Chem. Soc. Jpn.* **2007**, *80*, 677–685.
(37) Sadakane, M.; Asanuma, T.; Kubo, J.; Ueda, W. *Chem. Mater.* **2005**, *17*, 3546–3551.
(38) Yan, H.; Blanford, C. F.; Holland, B. T.; Smyrl, W. H.; Stein, A. *Chem. Mater.* **2000**, *12*, 1134–1141.
(39) Madhavi, S.; Ferraris, C.; White, T. *J. Solid State Chem.* **2006**, *179*, 866–872.
(40) Ergang, N. S.; Lytle, J. C.; Yan, H.; Stein, A. *J. Electrochem. Soc.* **2005**, *152*, A1989–A1995.
(41) Wang, C.; Geng, A.; Guo, Y.; Jiang, S.; Qu, X. *Mater. Lett.* **2006**, *60*, 2711–2714.
(42) Kim, I. D.; Rothschild, A.; Hyodo, T.; Tuller, H. L. *Nano Lett.* **2006**, *6*, 193–198.
(43) King, J. S.; Graugnard, E.; Summers, C. J. *Appl. Phys. Lett.* **2006**, *88*, 081109/1–081109/3.
(44) Ergang, N. S.; Lytle, J. C.; Lee, K. T.; Oh, S. M.; Smyrl, W. H.; Stein, A. *Adv. Mater.* **2006**, *18*, 1750–1753.
(45) Decher, G. *Science* **1997**, *227*, 1232–1237 and references therein.
(46) Caruso, F. *Adv. Mater.* **2001**, *13*, 11–22 and references therein.
(47) Wang, Z.; Ergang, N. S.; Al-Daous, M. A.; Stein, A. *Chem. Mater.* **2005**, *17*, 6805–6813.
(48) Yang, L.; Cao, W. *Chem. Mater.* **2006**, *18*, 297–300.
(49) Lodahl, P.; van Driel, A. F.; Nikolaev, I. S.; Irman, A.; Overgaag, K.; Vanmaekelbergh, D.; Vos, W. L. *Nature* **2004**, *430*, 654–657.
(50) Garcia, P. D.; Blanco, A.; Shavel, A.; Gaponik, N.; Eychmuller, A.; Rodriguez-Gonzalez, B.; Liz-Marzan, L. M.; Lopez, C. *Adv. Mater.* **2006**, *18*, 2768–2772.
(51) Dong, W.; Dong, H.; Wang, Z.; Zhan, P.; Yu, Z.; Zhao, X.; Zhu, Y.; Ming, N. *Adv. Mater.* **2006**, *18*, 755–759.
(52) Ding, S.; Qian, W.; Tan, Y.; Wang, Y. *Langmuir* **2006**, *22*, 7105–7108.
(53) Tan, Y.; Qian, W.; Ding, S.; Wang, Y. *Chem. Mater.* **2006**, *18*, 3385–3389.
(54) Chen, Z.; Gang, T.; Wang, Y.; Chen, X.; Guan, C.; Zhang, J.; Sun, Z.; Zhang, K.; Zhao, B.; Yang, B. *Colloids Surf., A* **2006**, *277*, 37–43.
(55) Ryu, J. H.; Chang, D. S.; Choi, B. G.; Yoon, J.-W.; Lim, C. S.; Shim, K. B. *Mater. Chem. Phys.* **2007**, *101*, 486–491.
(56) Busch, K.; John, S. *Phys. Rev. E: Stat., Nonlinear, Soft Matter Phys.* **1998**, *58*, 3896–3908.
(57) Doosje, M.; Hoenders, B. J.; Knoester, J. *J. Opt. Soc. Am. B* **2000**, *17*, 600–606.
(58) Dong, W.; Marlow, F. *Microporous Mesoporous Mater.* **2007**, *99*, 236–243.
(59) Chai, G. S.; Yoon, S. B.; Yu, J.-S.; Choi, J.-H.; Sung, Y.-E. *J. Phys. Chem. B* **2004**, *108*, 7074–7079.

(60) Han, S. E.; Stein, A.; Norris, D. J. *Phys. Rev. Lett.* **2007**, *99*, 053906/1–053906/4.

(61) Hung, D.; Liu, Z.; Shah, N.; Hao, Y.; Searson, P. C. *J. Phys. Chem. C* **2007**, *111*, 3308–3313.

(62) Aliev, A. E.; Lee, S. B.; Zakhidov, A. A.; Baughman, R. H. *Physica C (Amsterdam, Neth.)* **2007**, *453*, 15–23.

(63) Denny, N. R.; Han, S.; Turgeon, R. T.; Lytle, J. C.; Norris, D. J.; Stein, A. *SPIE Proc.* **2005**, *6005*, 60050501–60050513.

(64) Liu, B.; Jin, Z.; Qu, X.; Yang, Z. *Macromol. Rapid Commun.* **2007**, *28*, 322–328.

(65) Dong, W.; Bongard, H.; Tesche, B.; Marlow, F. *Adv. Mater.* **2002**, *14*, 1457–1460.

(66) Holland, B. T.; Blanford, C. F.; Do, T.; Stein, A. *Chem. Mater.* **1999**, *11*, 795–805.

(67) Dong, W.; Bongard, H. J.; Marlow, F. *Chem. Mater.* **2003**, *15*, 568–574.

(68) Zhong, Z.; Yin, Y.; Gates, B.; Xia, Y. *Adv. Mater.* **2000**, *12*, 206–209.

(69) Johnson, N. P.; McComb, D. W.; Richel, A.; Treble, B. M.; De La Rue, R. M. *Synth. Met.* **2001**, *116*, 469–473.

(70) Sokolov, S.; Bell, D.; Stein, A. *J. Am. Ceram. Soc.* **2003**, *86*, 1481–1486.

(71) Wijnhoven, J. E. G. J.; Bechger, L.; Vos, W. L. *Chem. Mater.* **2001**, *13*, 4486–4499.

(72) King, J. S.; Gaillot, D. P.; Graugnard, E.; Summers, C. J. *Adv. Mater.* **2006**, *18*, 1063–1067.

(73) Miguez, H.; Tetreault, N.; Yang, S. M.; Kitaev, V.; Ozin, G. A. *Adv. Mater.* **2003**, *15*, 597–600.

(74) Zukalova, M.; Kalbac, M.; Kavan, L. *Mater. Res. Soc. Symp. Proc.* **2004**, *820*, 363–368.

(75) Bartlett, P. N.; Dunford, T.; Ghanem, M. A. *J. Mater. Chem.* **2002**, *12*, 3130–3135.

(76) Graugnard, E.; King, J. S.; Gaillot, D. P.; Summers, C. J. *Adv. Funct. Mater.* **2006**, *16*, 1187–1196.

(77) Fenollosa, R.; Meseguer, F. *Adv. Mater.* **2003**, *15*, 1282–1285.

(78) Waterhouse, G. I. N.; Waterland, M. R. *Polyhedron* **2007**, *26*, 356–368.

(79) Wang, L.; Yan, Q.; Zhao, X. S. *J. Mater. Chem.* **2006**, *16*, 4598–4602.

(80) Li, J.; Zhang, Y. *Chem. Mater.* **2007**, *19*, 2581–2584.

(81) Yeo, S. H.; Teh, L. K.; Wong, C. C. *J. Porous Mater.* **2006**, *13*, 281–285.

(82) Chung, Y. W.; Leu, I. C.; Lee, J. H.; Yen, J. H.; Hon, M. H. *J. Electrochem. Soc.* **2007**, *154*, E77–E83.

(83) Sel, O.; Kuang, D.; Thommes, M.; Smarsly, B. *Langmuir* **2006**, *22*, 2311–2322.

(84) Yuan, Z. Y.; Su, B. L. *J. Mater. Chem.* **2006**, *16*, 663–677, and references therein.

(85) Su, B. L.; Vantomme, A.; Surahyyy, L.; Pirard, R.; Pirard, J. P. *Chem. Mater.* **2007**, *19*, 3325–3333.

(86) Cabanas, A.; Enciso, E.; Carbajo, M. C.; Torralvo, M. J.; Pando, C.; Renuncio, J. A. R. *Microporous Mesoporous Mater.* **2007**, *99*, 23–29.

(87) Wang, H.; Li, X. D.; Yu, F. C.; Kim, D. P. *Sci. China, Ser. E: Technol. Sci.* **2006**, *49*, 1–9.

(88) Antonietti, M.; Berton, B.; Göltner, C.; Hentze, H. P. *Adv. Mater.* **1998**, *10*, 154–159.

(89) Holland, B. T.; Abrams, L.; Stein, A. *J. Am. Chem. Soc.* **1999**, *121*, 4308–4309.

(90) Yin, J. S.; Wang, Z. L. *Appl. Phys. Lett.* **1999**, *74*, 2629–2631.

(91) Luo, Q.; Li, L.; Yang, B.; Zhao, D. *Chem. Lett.* **2000**, *378*, 379.

(92) Danumah, C.; Vaudreuil, S.; Bonneviot, L.; Bousmina, M.; Giasson, S.; Kaliaguine, S. *Microporous Mesoporous Mater.* **2001**, *44–45*, 241–247.

(93) Zhou, Y.; Antonietti, M. *Chem. Commun.* **2003**, *2564*, 2565.

(94) Sen, T.; Tiddy, G. J. T.; Casci, J. L.; Anderson, M. W. *Angew. Chem., Int. Ed.* **2003**, *42*, 4649–4653.

(95) Sen, T.; Tiddy, G. J. T.; Casci, J. L.; Anderson, M. W. *Chem. Mater.* **2004**, *16*, 2044–2054.

(96) Chai, G. S.; Shin, I. S.; Yu, J. S. *Adv. Mater.* **2004**, *16*, 2057–2061.

(97) Kuang, D.; Brezesinski, T.; Smarsly, B. *J. Am. Chem. Soc.* **2004**, *126*, 10534–10535.

(98) Villaescusa, L. A.; Mihi, A.; Rodriguez, I.; Garcia-Bennett, A. E.; Miguez, H. J. *J. Phys. Chem. B* **2005**, *109*, 19643–19649.

(99) Oh, C. G.; Baek, Y.; Ihm, S. K. *Adv. Mater.* **2005**, *17*, 270–273.

(100) Wang, Z.; Li, F.; Ergang, N. S.; Stein, A. *Chem. Mater.* **2006**, *18*, 5543–5553.

(101) Fujita, S.; Nakano, H.; Ishii, M.; Nakamura, H.; Inagaki, S. *Microporous Mesoporous Mater.* **2006**, *96*, 205–209.

(102) Kim, S. H.; Shin, C. K.; Ahn, C. H.; Kim, G. J. *J. Porous Mater.* **2006**, *13*, 201–205.

(103) Li, F.; Wang, Z.; Ergang, N. S.; Fyfe, C. A.; Stein, A. *Langmuir* **2007**, *23*, 3996–4004.

(104) Wang, Z.; Stein, A. *Chem. Mater.* **2008**, *20*, [online] DOI: 10.1021/cm0717864.

(105) Woo, S.-W.; Dokko, K.; Sasajima, K.; Takei, T.; Kanamura, K. *Chem. Commun.* **2006**, *4099*, 4101.

(106) Deng, Y.; Liu, C.; Yu, T.; Liu, F.; Zhang, F.; Wan, Y.; Zhang, L.; Wang, C.; Tu, B.; Webley, P. A.; Wang, H.; Zhao, D. *Chem. Mater.* **2007**, *19*, 3271–3277.

(107) Hu, X.; An, Q.; Li, G.; Tao, S.; Liu, J. *Angew. Chem., Int. Ed.* **2006**, *45*, 8145–8148.

(108) Yang, S. M.; Coombs, N.; Ozin, G. A. *Adv. Mater.* **2000**, *12*, 1940–1944.

(109) Jiang, P.; Bertone, J. F.; Colvin, V. L. *Science* **2001**, *291*, 453–457.

(110) Xu, L.; Tung, L. D.; Spinu, L.; Zakhidov, A. A.; Baughman, R. H.; Wiley, J. B. *Adv. Mater.* **2003**, *15*, 1562–1564.

(111) Wang, H.; Yu, J.-S.; Li, X.-D.; Kim, D.-P. *Chem. Commun.* **2004**, *2352*, 2353.

(112) Cong, H.; Cao, W. *Solid State Sci.* **2006**, *8*, 1056–1060.

(113) Rong, J.; Liu, S.; Liu, Y. *Polymer* **2006**, *47*, 2677–2682.

(114) Li, F.; Wang, Z.; Stein, A. *Angew. Chem., Int. Ed.* **2007**, *46*, 1885–1888.

(115) Li, F.; Delo, S. A.; Stein, A. *Angew. Chem., Int. Ed.* **2007**, *46*, 6666–6669.

(116) Li, F.; Stein, A. Unpublished results, 2007.

(117) Wang, Z.; Li, F.; Stein, A. *Nano Lett.* **2007**, *7*, 3223–3226.

(118) Schüth, F.; Marlow, F. *Nature* **2007**, *449*, 550–551.

(119) Lytle, J. C.; Yan, H.; Turgeon, R. T.; Stein, A. *Chem. Mater.* **2004**, *16*, 3829–3837.

(120) Cho, Y. S.; Yi, G. R.; Kim, S. H.; Jeon, S. J.; Elsesser, M. T.; Yu, H. K.; Yang, S. M.; Pine, D. J. *Chem. Mater.* **2007**, *19*, 3183–3193.

(121) Iskander, F.; Nandiyanto, A. B. D.; Yun, K. M.; Hogan, J. C. J.; Okuyama, K.; Biswas, P. *Adv. Mater.* **2007**, *19*, 1408–1412.

(122) Kim, S.-H.; Lee, S. Y.; Yi, G.-R.; Pine, D. J.; Yang, S.-M. *J. Am. Chem. Soc.* **2006**, *128*, 10897–10904.

(123) Li, H.; Wang, H.; Chen, A.; Meng, B.; Li, X. *J. Mater. Chem.* **2005**, *15*, 2551–2556.

(124) Kuncicky, D. M.; Bose, K.; Costa, K. D.; Velev, O. D. *Chem. Mater.* **2007**, *19*, 141–143.

(125) Beh, W. S.; Xia, Y.; Qin, D. *J. Mater. Res.* **1999**, *14*, 3995–4003.

(126) Ozin, G. A.; Yang, S. M. *Adv. Funct. Mater.* **2001**, *11*, 95–104.

(127) Wang, H.; Li, X.; Hong, L.-Y.; Kim, D.-P. *J. Porous Mater.* **2006**, *13*, 115–121.

(128) Kuo, C. Y.; Lu, S. Y. *J. Am. Ceram. Soc.* **2007**, *90*, 1956–1958.

(129) Vekris, E.; Ozin, G. A.; Kitaev, V. *Adv. Mater.* **2006**, *18*, 2481–2485.

(130) Lu, C.; Qi, L.; Cong, H.; Wang, X.; Yang, J.; Yang, L.; Zhang, D.; Ma, J.; Cao, W. *Chem. Mater.* **2005**, *17*, 5218–5224.

(131) Wucher, B.; Yue, W.; Kulak, A. N.; Meldrum, F. C. *Chem. Mater.* **2007**, *19*, 1111–1119.

(132) Wegner, G.; Baum, P.; Mueller, M.; Norwig, J.; Landfester, K. *Macromol. Symp.* **2001**, *175*, 349–355.

(133) Liu, Z.; Jin, Z.; Li, W.; Liu, X.; Qiu, J.; Wu, W. *Mater. Lett.* **2006**, *60*, 810–814.

(134) Fu, M.; Zhou, J.; Xiao, Q.; Li, B.; Zong, R.; Chen, W.; Zhang, J. *Adv. Mater.* **2006**, *18*, 1001–1004.

(135) Kamp, U.; Kitaev, V.; von Freymann, G.; Ozin, G. A.; Mabary, S. *Adv. Mater.* **2005**, *17*, 438–443.

(136) Li, F.; He, J.; Zhou, W. L.; Wiley, J. B. *J. Am. Chem. Soc.* **2003**, *125*, 16166–16167.

(137) Wang, X.; Bozhilov, K. N.; Feng, P. *Chem. Mater.* **2006**, *18*, 6373–6381.

(138) Lee, K. T.; Lytle, J. C.; Ergang, N. S.; Oh, S. M.; Stein, A. *Adv. Funct. Mater.* **2005**, *15*, 547–556.

(139) Denny, N. R.; Han, S. E.; Norris, D. J.; Stein, A. *Chem. Mater.* **2007**, *19*, 4563–4569.

(140) Blanco, A.; Lopez, C. Photonic Crystals: Fundamentals and Applications. In *Annual Review of Nanoresearch*; Cao, G., Brinker, C. J., Eds.; World Scientific: Singapore, 2006; Vol. 1, pp 81–152.

(141) Toader, O.; John, S. *Phys. Rev. E: Stat., Nonlinear, Soft Matter Phys.* **2004**, *70*, 046605/1–046605/15.

(142) Aryal, D. P.; Jamois, C.; Hermann, C.; Hess, O. *SPIE Proc.* **2005**, *5950*, 59500Y/1–59500Y/6.

(143) Gaillot, D.; Yamashita, T.; Summers, C. J. *Phys. Rev. B: Condens. Matter Mater. Phys.* **2005**, *72*, 205109/1–205109/10.

(144) Dong, W.; Marlow, F. *Physica E (Amsterdam, Neth.)* **2003**, *17*, 431–432.

(145) Blanco, A.; Chomski, E.; Grabtchak, S.; Ibisate, M.; John, S.; Leonard, S. W.; Lopez, C.; Meseguer, F.; Miguez, H.; Mondia, J. P.; Ozin, G. A.; Toader, O.; van Driel, H. M. *Nature* **2000**, *405*, 437–440.

(146) Vlasov, Y. A.; Bo, X. Z.; Sturm, J. C.; Norris, D. J. *Nature* **2001**, *414*, 289–293.

(147) Juarez, B. H.; Ibisate, M.; Palacios, J. M.; Lopez, C. *Adv. Mater.* **2003**, *15*, 319–323.

(148) Becker, C.; Linden, S.; von Freymann, G.; Wegener, M.; Tetreault, N.; Vekris, E.; Kitaev, V.; Ozin, G. A. *Appl. Phys. Lett.* **2005**, *87*, 091111/1–091111/3.

(149) Ni, P.; Cheng, B.; Zhang, D. *Appl. Phys. Lett.* **2002**, *80*, 1879–1881.

(150) Vos, W. L.; Polman, A. *MRS Bull.* **2001**, *26*, 642–646.

(151) Schriemer, H. P.; van Driel, H. M.; Koenderink, A. F.; Vos, W. L. *Phys. Rev. A: At., Mol., Opt. Phys.* **2001**, *63*, 011801/1–011801/4.

(152) Romanov, S. G.; Maka, T.; Sotomayor Torres, C. M.; Muller, M.; Zentel, R. *Appl. Phys. Lett.* **2001**, *79*, 731–733.

(153) Koenderink, A. F.; Bechger, L.; Lagendijk, A.; Vos, W. L. *Phys. Status Solidi A* **2003**, *197*, 648–661.

(154) Solovyev, V. G.; Romanov, S. G.; Sotomayor Torres, C. M.; Muller, M.; Zentel, R.; Gaponik, N.; Eychmuller, A.; Rogach, A. L. *J. Appl. Phys.* **2003**, *94*, 1205–1210.

(155) Bechger, L.; Lodahl, P.; Vos, W. L. *J. Phys. Chem. B* **2005**, *109*, 9980–9988.

(156) Schroden, R. C.; Al-Daous, M.; Stein, A. *Chem. Mater.* **2001**, *13*, 2945–2950.

(157) Kayashima, H.; Sumioka, K.; Lee, S. H.; Jang, B.-B.; Fujita, K.; Tsutsui, T. *Jpn. J. Appl. Phys., Part 1* **2003**, *42*, 5731–5734.

(158) Scharrer, M.; Wu, X.; Yamilov, A.; Cao, H.; Chang, R. P. H. *Appl. Phys. Lett.* **2005**, *86*, 151113/1–151113/3.

(159) Yang, Y.; Yan, H.; Fu, Z.; Yang, B.; Xia, L.; Xu, Y.; Zuo, J.; Li, F. *J. Phys. Chem. B* **2006**, *110*, 846–852.

(160) Hermann, C.; Hess, O. *J. Opt. Soc. Am. B* **2002**, *19*, 3013–3018.

(161) Chen, J. I. L.; von Freymann, G.; Choi, S. Y.; Kitaev, V.; Ozin, G. A. *Adv. Mater.* **2006**, *18*, 1915–1919.
(162) Nishimura, S.; Abrams, N.; Lewis, B. A.; Halaoui, L. I.; Mallouk, T. E.; Benkstein, K. D.; Van De Lagemaat, J.; Frank, A. J. *J. Am. Chem. Soc.* **2003**, *125*, 6306–6310.
(163) Halaoui, L. I.; Abrams, N. M.; Mallouk, T. E. *J. Phys. Chem. B* **2005**, *109*, 6334–6342.
(164) Somani, P. R.; Dionigi, C.; Murgia, M.; Palles, D.; Nozar, P.; Ruani, G. *Sol. Energy Mater. Sol. Cells* **2005**, *87*, 513–519.
(165) Huisman, C. L.; Schoonman, J.; Goossens, A. *Sol. Energy Mater. Sol. Cells* **2005**, *85*, 115–124.
(166) Rodriguez, I.; Ramiro-Manzano, F.; Atienzar, P.; Martinez, J. M.; Meseguer, F.; Garcia, H.; Corma, A. *J. Mater. Chem.* **2007**, *17*, 3205–3209.
(167) Chen, J. I. L.; von Freymann, G.; Kitaev, V.; Ozin, G. A. *J. Am. Chem. Soc.* **2007**, *129*, 1196–1202.
(168) Li, X.; Tao, F.; Jiang, Y.; Xu, Z. *J. Colloid Interface Sci.* **2007**, *308*, 460–465.
(169) Li, Z. Y.; Zhang, Z. Q. *Phys. Rev. B: Condens. Matter Mater. Phys.* **2000**, *62*, 1516–1519.
(170) Biswas, R.; Sigalas, M. M.; Subramania, G.; Soukoulis, C. M.; Ho, K. M. *Phys. Rev. B: Condens. Matter Mater. Phys.* **2000**, *61*, 4549–4553.
(171) Vlasov, Y. A.; Deutsch, M.; Norris, D. J. *Appl. Phys. Lett.* **2000**, *76*, 1627–1629.
(172) D'Andrea, A.; Pilozzi, L.; Schiumarini, D.; Tomassini, N. *SPIE Proc.* **2003**, *5036*, 424–429.
(173) Sinitskii, A.; Abramova, V.; Laptinskaya, T.; Tretyakov, Y. D. *Phys. Lett. A* **2007**, *366*, 516–522.
(174) Shimmin, R. G.; Vajtai, R.; Siegel, R. W.; Braun, P. V. *Chem. Mater.* **2007**, *19*, 2102–2107.
(175) Wang, L.; Yan, Q.; Zhao, X. S. *Langmuir* **2006**, *22*, 3481–3484.
(176) Lee, W.; Pruzinsky, S. A.; Braun, P. V. *Adv. Mater.* **2002**, *14*, 271–274.
(177) Lange, B.; Wagner, J.; Zentel, R. *Macromol. Rapid Commun.* **2006**, *27*, 1746–1751.
(178) Lange, B.; Jhaveri, S. J.; Steidl, L.; Ayothi, R.; Ober, C. K.; Zentel, R. *Macromol. Rapid Commun.* **2007**, *28*, 922–926.
(179) Li, B.; Zhou, J.; Li, L.; Wang, X. J.; Liu, X. H.; Jian, Z. *Appl. Phys. Lett.* **2003**, *83*, 4704–4706.
(180) Kuai, S.-L.; Bader, G.; Ashrit, P. V. *Appl. Phys. Lett.* **2005**, *86*, 221110/1–221110/3.
(181) Asher, S. A.; Holtz, J.; Weissman, J.; Pan, G. S. *MRS Bull.* **1998**, *23*, 44–50.
(182) Lee, Y.-J.; Braun, P. V. *Adv. Mater.* **2003**, *15*, 563–566.
(183) Lee, Y.-J.; Pruzinsky, S. A.; Braun, P. V. *Langmuir* **2004**, *20*, 3096–3106.
(184) Barry, R. A.; Wiltzius, P. *Langmuir* **2006**, *22*, 1369–1374.
(185) Matsubara, K.; Watanabe, M.; Takeoka, Y. *Angew. Chem., Int. Ed.* **2007**, *46*, 1688–1692.
(186) Lee, Y.-J.; Heitzman, C. E.; Frei, W. R.; Johnson, H. T.; Braun, P. V. *J. Phys. Chem. B* **2006**, *110*, 19300–19306.
(187) Arsenault, A. C.; Clark, T. J.; von Freymann, G.; Cademartiri, L.; Sapienza, R.; Bertolotti, J.; Vekris, E.; Wong, S.; Kitaev, V.; Manners, I.; Wang, R. Z.; John, S.; Wiersma, D.; Ozin, G. A. *Nat. Mater.* **2006**, *5*, 179–184.
(188) Sumioka, K.; Kayashima, H.; Tsutsui, T. *Adv. Mater.* **2002**, *14*, 1284–1286.
(189) Babin, V.; Garstecki, P.; Holyst, R. *Appl. Phys. Lett.* **2003**, *82*, 1553–1555.
(190) Kuo, C. Y.; Lu, S. Y.; Chen, S.; Bernards, M.; Jiang, S. *Sens. Actuators, B* **2007**, *124*, 452–458.
(191) Ozaki, M.; Shimoda, Y.; Kasano, M.; Yoshino, K. *Adv. Mater.* **2002**, *14*, 514–518.
(192) Mach, P.; Wiltzius, P.; Megens, M.; Weitz, D. A.; Lin, K.-h.; Lubensky, T. C.; Yodh, A. G. *Phys. Rev. E: Stat., Nonlinear, Soft Matter Phys.* **2002**, *65*, 031720/1–031720/3.
(193) Kubo, S.; Gu, Z.-Z.; Takahashi, K.; Fujishima, A.; Segawa, H.; Sato, O. *J. Am. Chem. Soc.* **2004**, *126*, 8314–8319.
(194) Kubo, S.; Gu, Z.-Z.; Takahashi, K.; Fujishima, A.; Segawa, H.; Sato, O. *Chem. Mater.* **2005**, *17*, 2298–2309.
(195) Graugnard, E.; King, J. S.; Jain, S.; Summers, C. J.; Zhang-Williams, Y.; Khoo, I. C. *Phys. Rev. B: Condens. Matter Mater. Phys.* **2005**, *72*, 233105/1–233105/4.
(196) Moritsugu, M.; Kim, S. N.; Ogata, T.; Nonaka, T.; Kurihara, S.; Kubo, S.; Segawa, H.; Sato, O. *Appl. Phys. Lett.* **2006**, *89*, 153131/1–153131/3.
(197) Ruhl, T.; Spahn, P.; Hermann, C.; Jamois, C.; Hess, O. *Adv. Funct. Mater.* **2006**, *16*, 885–890.
(198) Kumoda, M.; Watanabe, M.; Takeoka, Y. *Langmuir* **2006**, *22*, 4403–4407.
(199) Krivorotov, I. N.; Yan, H.; Dan Dahlberg, E.; Stein, A. *J. Magn. Magn. Mater.* **2001**, *226–230*, 1800–1802.
(200) Bartlett, P. N.; Ghanem, M. A.; El Hallag, I. S.; De Groot, P.; Zhukov, A. *J. Mater. Chem.* **2003**, *13*, 2596–2602.
(201) Zhukov, A. A.; Goncharov, A. V.; de Groot, P. A. J.; Bartlett, P. N.; Ghanem, M. A. *J. Appl. Phys.* **2003**, *93*, 7322–7324.
(202) Eagleton, T. S.; Searson, P. C. *Chem. Mater.* **2004**, *16*, 5027–5032.
(203) Hao, Y.; Zhu, F. Q.; Chien, C. L.; Searson, P. C. *J. Electrochem. Soc.* **2007**, *154*, D65–D69.
(204) Galloro, J.; Ginzburg, M.; Miguez, H.; Yang, S. M.; Coombs, N.; Safa-Sefat, A.; Greedan, J. E.; Manners, I.; Ozin, G. A. *Adv. Funct. Mater.* **2002**, *12*, 382–388.
(205) Gu, Z.-Z.; Uetsuka, H.; Takahashi, K.; Nakajima, R.; Onishi, H.; Fujishima, A.; Sato, O. *Angew. Chem., Int. Ed.* **2003**, *42*, 894–897.
(206) Li, Y.; Cai, W.; Cao, B.; Duan, G.; Sun, F.; Li, C.; Jia, L. *Nanotechnology* **2006**, *17*, 238–243.
(207) Li, J.; Fu, J.; Cong, Y.; Wu, Y.; Xue, L.; Han, Y. *Appl. Surf. Sci.* **2006**, *252*, 2229–2234.
(208) Ge, H.; Wang, G.; He, Y.; Wang, X.; Song, Y.; Jiang, L.; Zhu, D. *ChemPhysChem* **2006**, *7*, 575–578.
(209) Sakamoto, J. S.; Dunn, B. *J. Mater. Chem.* **2002**, *12*, 2859–2861.
(210) Yan, H.; Sokolov, S.; Lytle, J. C.; Stein, A.; Zhang, F.; Smyrl, W. H. *J. Electrochem. Soc.* **2003**, *150*, A1102–A1107.
(211) Lytle, J. C.; Yan, H.; Ergang, N.; Smyrl, W. H.; Stein, A. *J. Mater. Chem.* **2004**, *14*, 1616–1622.
(212) Lu, J.; Tang, Z.; Zhang, Z.; Shen, W. *Mater. Res. Bull.* **2005**, *40*, 2039–2046.
(213) Wang, C.; Yang, C.; Song, Y.; Gao, W.; Xia, X. *Adv. Funct. Mater.* **2005**, *15*, 1267–1275.
(214) Su, F.; Zhao, X. S.; Wang, Y.; Zeng, J.; Zhou, Z.; Lee, J. Y. *J. Phys. Chem. B* **2005**, *109*, 20200–20206.
(215) Moriguchi, I.; Nakawara, F.; Yamada, H.; Kudo, T. *Stud. Surf. Sci. Catal.* **2005**, *156*, 589–594.
(216) Tian, S.; Wang, J.; Jonas, U.; Knoll, W. *Chem. Mater.* **2005**, *17*, 5726–5730.
(217) Sorensen, E. M.; Barry, S. J.; Jung, H. K.; Rondinelli, J. R.; Vaughey, J. T.; Poeppelmeier, K. R. *Chem. Mater.* **2006**, *18*, 482–489.
(218) Bing, Z.; Yuan, Y.; Wang, Y.; Fu, Z.-W. *Electrochem. Solid-State Lett.* **2006**, *9*, A101–A104.
(219) Yamada, H.; Nakamura, H.; Nakahara, F.; Moriguchi, I.; Kudo, T. *J. Phys. Chem. C* **2007**, *111*, 227–233.
(220) Yamada, H.; Tagawa, K.; Komatsu, M.; Moriguchi, I.; Kudo, T. *J. Phys. Chem. C* **2007**, *111*, 8397–8402.
(221) Reculusa, S.; Agricole, B.; Derre, A.; Couzi, M.; Sellier, E.; Ravaine, S.; Delhaes, P. *Adv. Mater.* **2006**, *18*, 1705–1708.
(222) Reculusa, S.; Agricole, B.; Derre, A.; Couzi, M.; Sellier, E.; Delhaes, P.; Ravaine, S. *Electroanalysis* **2007**, *19*, 379–384.
(223) Lai, C. Z.; Fierke, M. A.; Stein, A.; Bühlmann, P. *Anal. Chem.* **2007**, *79*, 4621–4626.
(224) Munakata, H.; Chiba, H.; Dokko, K.; Hamagami, J. I.; Takei, T.; Kanamura, K. *Key Eng. Mater.* **2006**, *301*, 143–146.
(225) Munakata, H.; Yamamoto, D.; Dokko, K.; Hamagami, J.-i.; Takei, T.; Kanamura, K. *Proc. Electrochem. Soc.* **2006**, *2004–21*, 252–258.
(226) Wang, C.; Yang, C.; Song, Y.; Gao, W.; Xia, X. *Adv. Funct. Mater.* **2005**, *15*, 1267–1275.
(227) Szamocki, R.; Reculusa, S.; Ravaine, S.; Bartlett, P. N.; Kuhn, A.; Hempelmann, R. *Angew. Chem., Int. Ed.* **2006**, *45*, 1317–1321.
(228) Szamocki, R.; Velichko, A.; Holzapfel, C.; Muecklich, F.; Ravaine, S.; Garrigue, P.; Sojic, N.; Hempelmann, R.; Kuhn, A. *Anal. Chem.* **2007**, *79*, 533–539.
(229) Liu, Y.; Wang, S. *Colloids Surf., B* **2007**, *58*, 8–13.
(230) Sung, I. K.; Christian; Mitchell, M.; Kim, D. P.; Kenis, P. J. A. *Adv. Funct. Mater.* **2005**, *15*, 1336–1342.
(231) Mitchell, M.; Kim, D. P.; Kenis, P. J. A. *J. Catal.* **2006**, *241*, 235–242.
(232) Guan, G.; Zapf, R.; Kolb, G.; Men, Y.; Hessel, V.; Loewe, H.; Ye, J.; Zentel, R. *Chem. Commun.* **2007**, *260*, 262.
(233) Yin, Y.; Xia, Y. *Adv. Mater.* **2001**, *13*, 267–271.
(234) Manoharan, V. N.; Elsesser, M. T.; Pine, D. J. *Science* **2003**, *301*, 483–487.
(235) Hoogenboom, J. P.; Retif, C.; de Bres, E.; van de Boer, M.; Van Langen-Suurling, A. K.; Romijn, J.; van Blaaderen, A. *Nano Lett.* **2004**, *4*, 205–208.
(236) Leunissen, M. E.; Christova, C. G.; Hynninen, A. P.; Royall, C. P.; Campbell, A. I.; Imhof, A.; Dijkstra, M.; van Roij, R.; van Blaaderen, A. *Nature* **2005**, *437*, 235–240.
(237) Jin, C.; Li, Z.-Y.; McLachlan, M. A.; McComb, D. W.; De La Rue, R. M.; Johnson, N. P. *J. Appl. Phys.* **2006**, *99*, 116109/1–116109/3.
(238) Velev, O. D. *Science* **2006**, *312*, 376–377.

CM702107N